

PACIFIC EARTHQUAKE ENGINEERING RESEARCH CENTER

Seismic Response of a Hybrid Fiber-Reinforced Concrete Bridge Column Detailed for Accelerated Bridge Construction

**Wilson Nguyen
William Trono
Marios Panagiotou
Claudia P. Ostertag**

Department of Civil and Environmental Engineering
University of California, Berkeley

Disclaimer

The opinions, findings, and conclusions or recommendations expressed in this publication are those of the author(s) and do not necessarily reflect the views of the study sponsor(s) or the Pacific Earthquake Engineering Research Center.

Seismic Response of a Hybrid Fiber-Reinforced Concrete Bridge Column Detailed for Accelerated Bridge Construction

**Wilson Nguyen
William Trono
Marios Panagiotou
Claudia P. Ostertag**

Department of Civil and Environmental Engineering
University of California, Berkeley

PEER Report 2014/19
Pacific Earthquake Engineering Research Center
Headquarters at the University of California, Berkeley
December 2014

ABSTRACT

With the expected rehabilitation and replacement of damaged reinforced concrete bridges to occur in the next several decades, an opportunity exists to design bridge columns that have an accelerated construction schedule, which would reduce costs related to traffic closures and productivity loss, and to design columns that exhibit enhanced crack resistance, which would reduce damage from seismic events and long-term environmental degradation. This study investigates the feasibility of using a precast hybrid fiber-reinforced concrete (HyFRC) tube element as the exterior shell of a bridge column, which then has its hollow core filled with plain concrete once cast within a foundation. By isolating the fiber-reinforced concrete casting in the precast phase, fabrication of the tube element becomes a well-controlled process, alleviating concerns about the reduced cast-in-place workability associated with fiber-reinforced concrete, and allowing the column to take advantage of the fibers' enhancement to concrete mechanical properties.

The 1:4.5 scaled tube column had a longitudinal steel ratio of 1.2% and volumetric transverse steel ratio of 0.87%. To accommodate nonlinear deformations, the column utilized a rocking behavior at its base by unbonding the column's longitudinal reinforcement from the concrete near the base.

The seismic performance of the column was evaluated after subjecting it to static uni-directional cyclic loading. The column was able to withstand drift ratios as high as 13.1% without losing axial load capacity, and longitudinal rebar did not fracture up to drift ratios of 9.5%. Compression damage of the column was relatively low by the end of the test, as spalling of concrete cover was not witnessed. Compared to a similarly sized rocking column cast entirely with hybrid fiber-reinforced concrete, the tube column maintained a higher lateral load capacity at large drift ratios, and had less observed structural damage.

ACKNOWLEDGMENTS

This work was supported by the State of California through the Transportation System Research Program of the Pacific Earthquake Engineering Research Centers (PEER). Any opinions, findings, and conclusions or recommendations expressed in this material are those of the authors and do not necessarily reflect those of the funding agency.

We would like to thank Joel Carr, Lev Stepanov, Philip Wong, Jeff Higginbotham, and Matt Cataleta for their help in preparing and conducting the experiments.

CONTENTS

ABSTRACT	iii
ACKNOWLEDGMENTS	v
TABLE OF CONTENTS	vii
LIST OF TABLES	ix
LIST OF FIGURES	xi
1 INTRODUCTION	1
1.1 Motivation for Accelerated Bridge Construction (ABC)	1
1.2 Motivation for Using Hybrid Fiber-Reinforced Concrete (HyFRC)	2
1.3 HyFRC in Bridge Columns	3
1.4 Research Objectives	4
1.5 Organization of the Report	5
2 SPECIMEN DESIGN AND CONSTRUCTION	7
2.1 Design of Column	7
2.1.1 Details of Prototype Column	7
2.1.2 Structural Details of Tube Column	8
2.2 Materials Used in Construction	10
2.2.1 Precast Tube HyFRC	10
2.2.2 Core Concrete	14
2.2.3 Steel.....	14
2.3 Construction of Test Specimen	15
2.3.1 Precast Tube.....	15
2.3.2 Foundation and Column Core.....	17
3 EXPERIMENTAL SET-UP AND TEST PROGRAM	21
3.1 Test Set-Up	21
3.2 Data Instrumentation	22
3.3 Loading Protocol	25

4	EXPERIMENTAL RESULTS AND DISCUSSION.....	27
4.1	Lateral Force-Displacement Response.....	27
4.2	Rocking Behavior.....	29
4.3	Compression Damage.....	34
4.4	Comparison to Cast-in-Place Columns.....	37
5	SUMMARY AND CONCLUSIONS	41
	REFERENCES.....	43
APPENDIX A	COLUMN MIX DESIGNS.....	45
APPENDIX B	RESPONSE HISTORY OF VERTICAL DISPLACEMENT TRANSDUCERS AND STRAIN GAUGES.....	47

LIST OF TABLES

Table 2.1	Comparison of column gross dimensions.....	8
Table 2.2	Comparison of column concrete type and steel reinforcement.....	8
Table 2.3	Comparison of baseline and finalized saturated surface dry (SSD) proportions for tube HyFRC.....	11
Table 2.4	Fiber properties.....	11
Table 2.5	Compression test results of tube HyFRC after 73 days.....	14
Table 2.6	Bending test results of tube HyFRC after 73 days.....	14
Table 2.7	Summary of steel used in specimen.....	14
Table 3.1	Number of cycles at target drift ratios ($H = 65.00$ in.).....	26
Table A.1	Tube HyFRC SSD Mix Proportions (1 yd^3).....	45
Table A.2	Tube HyFRC SSD Mix Proportion Ratios.....	45
Table A.3	Tube HyFRC batched mix proportions (0.33 yd^3).....	46
Table A.4	Core concrete SSD mix proportions (1 yd^3).....	46
Table A.5	Core concrete SSD mix proportion ratios.....	46
Table A.6	Core concrete batched mix proportions (0.20 yd^3).....	46

LIST OF FIGURES

Figure 1.1	Schematic of crack-fiber interactions: (a) FRC with macrofibers only; and (b) HyFRC with micro- and macrofibers.....	2
Figure 2.1	Elevation view and cross section of prototype bridge column [Ketchum et al. 2004].	7
Figure 2.2	Tube column structural details. Steel pipe corrugations and foundation details not shown, for clarity.	9
Figure 2.3	Slump flow test of tube HyFRC.....	12
Figure 2.4	Tube HyFRC compression test results.....	13
Figure 2.5	Tube HyFRC beam bending test results.	13
Figure 2.6	Steel reinforcement tensile test results: (a) longitudinal steel; and (b) spiral steel.....	15
Figure 2.7	Elevation photographs of tube construction: (a) full elevation view; and (b) close up at unbonded region in tube.	16
Figure 2.8	Detail photographs of tube construction: (a) unbonded rebar through use of duct tape within lower 18 in. of tube; and (b) plan view of tube cross section at top opening.	17
Figure 2.9	Elevation photographs of tube installment into foundation: (a) tube before installation; (b) tube aligned into foundation rebar cage; and (c) tube cast within foundation.	18
Figure 2.10	Detail photographs of tube installment into foundation: (a) close up at tube base, showing extruded longitudinal rebar from tube; and (b) extruded longitudinal rebar from tube within foundation rebar cage.	18
Figure 2.11	Top view of column prior to core casting.	19
Figure 3.1	Global view photograph of test set-up.	21
Figure 3.2	Detail photograph of horizontal actuators.....	22
Figure 3.3	Location of strain gauges on longitudinal rebar. Section A-A shows rebar designation. (*) refers to rebar with strain gauges. Elevation view shows 1 rebar for clarity; units in inches.	23
Figure 3.4	Locations of West and East face displacement transducers; units in inches.	23
Figure 3.5	Locations of north and south face displacement transducers; units in inches.	24

Figure 3.6	Detail photographs of displacement transducers: (a) East column face; and (b) North column face.	24
Figure 3.7	Actual lateral drift ratios applied.	25
Figure 4.1	Complete lateral load-drift ratio response. Circle markers indicate points of longitudinal rebar fracture.	28
Figure 4.2	Lateral load-drift ratio response to $\theta_r = 4.8\%$	28
Figure 4.3	Northeast face of column at neutral position: (a) $\theta_r = 0.60\%$; (b) $\theta_r = 2.4\%$; (c) $\theta_r = 6.0\%$; and (d) $\theta_r = 11.3\%$	29
Figure 4.4	West face of column at neutral position: (a) $\theta_r = 0.60\%$; (b) $\theta_r = 2.4\%$; (c) $\theta_r = 6.0\%$; and (d) $\theta_r = 11.3\%$	30
Figure 4.5	Elevation view of column: (a) West face in extreme tension, $\theta_r = 2.4\%$; and (b) East face in neutral position, $\theta_r = 2.4\%$	30
Figure 4.6	Column during extreme eastern drift, at $\theta_r = 11.3\%$: (a) global view, viewing from southern side; and (b) close-up at western face, viewing from northern side, showing exposed longitudinal rebar.	31
Figure 4.7	Displacement versus drift ratio based on column base displacement transducer measurements from DT-W-1 and DT-E-1.	32
Figure 4.8	Column base rotation versus drift ratio, based on column base displacement measurements from DT-W-1 and DT-E-1. The dashed diagonal line represents perfectly rigid column movement.	32
Figure 4.9	Strain gauge measurements as a function of data steps at the middle and top positions for longitudinal rebar 2, 3, 6, and 7. Vertical line intervals indicate the completion of a target drift ratio cyclic sequence.	33
Figure 4.10	East face of column at neutral position, $\theta_r = 8.3\%$. Permanent vertical displacement can be observed between the column–foundation interface.	34
Figure 4.11	Residual vertical displacements.	34
Figure 4.12	Southeast face of column at extreme eastward loading: (a) $\theta_r = 4.8\%$; (b) $\theta_r = 6.0\%$; (c) $\theta_r = 9.5\%$; and (d) $\theta_r = 11.1\%$	35
Figure 4.13	Northwest face of column at extreme westward loading: (a) $\theta_r = 8.3\%$; and (b) $\theta_r = 9.5\%$	36
Figure 4.14	West spiral and East spiral strain gauge measurements.	36
Figure 4.15	Extreme compressive strain profile based on displacement transducer measurements.	37
Figure 4.16	Complete lateral load-drift ratio response of tube column and TS-1. Circle markers indicate points of longitudinal rebar fracture.	38

Figure 4.17	Lateral load-drift ratio response of tube column and TS-1, to $\theta_r=4.8\%$	38
Figure 4.18	Complete lateral load-drift ratio response of tube column and TS-1, with global envelope curve shown for clarity.....	39
Figure 4.19	Column compression damage: (a) Tube column at 4.8% drift; fine splitting cracks are present on the column surface; (b) TS-1 after 4.8% drift; localized buckling at fabrication flaw is highlighted [Kumar et al. 2011]; and (c) Base45 after 4.0% drift; spalling is extensive at the column base [Terzic and Stojadinovic 2010].....	40
Figure B.1	Displacement transducer measurements on western and eastern column faces. <i>X</i> -axis is in drift ratio (%); <i>Y</i> -axis is in displacement (in.).....	47
Figure B.2	Displacement transducer measurements on northern and southern column faces. <i>X</i> -axis is in drift ratio (%); <i>Y</i> -axis is in displacement (in.).....	48
Figure B.3	Strain gauge measurements from column west face rebar. <i>X</i> -axis is in drift ratio (%); <i>Y</i> -axis is in strain (in./in.).....	49
Figure B.4	Strain gauge measurements from column east face rebar. <i>X</i> -axis is in drift ratio (%); <i>Y</i> -axis is in strain (in./in.). Measurements from SG-B5 were not obtained.....	50

1 Introduction

1.1 MOTIVATION FOR ACCELERATED BRIDGE CONSTRUCTION (ABC)

The deterioration of reinforced concrete bridges is a major durability and economic problem in the U.S. In a 2013 study conducted by the American Society of Civil Engineers (ASCE), approximately one-fourth of the 600,000 bridges in the U.S. were rated as structurally deficient or functionally obsolete, requiring rehabilitation or complete replacement [American Society of Civil Engineers 2013]. While repairing or constructing new bridges has direct costs associated with materials and labor, indirect costs related to unproductivity caused by partial or total bridge closures may exceed all direct costs, potentially affecting local economy. Bridge construction in metropolitan areas is especially troublesome, as millions of daily commuters and freighters may be affected. The Federal Highway Administration (FHWA) estimates an annual cost of \$20.5 billion is required to clear the nation of deficient bridges by 2028.

Due to the significant influence of time on the overall cost of bridge projects, novel designs aimed at expediting construction methods may be worthwhile alternatives to more conventional designs. Such an approach may be generalized as accelerated bridge construction (ABC). By systematically reducing construction time periods, several desired outcomes can be achieved, such as the aforementioned reduction in costs due to onsite construction time, as well as reductions in temporary structures, improved worker safety, and reduced dependency on weather conditions [Culmo 2011].

The use of precast bridge elements and systems, which calls for structural components of a bridge to be fabricated offsite, is a manner of incorporating ABC methods into a project. In the case of reinforced concrete bridges, expedition in schedule may result from reduction in, or elimination of, onsite rebar assembly, curing time due to cast-in-place concrete pouring, and formwork removal. A variety of precast concrete systems exist, as detailed by Hieber et al. [2005]. In particular, bridge columns are of interest. During a seismic event, the columns are typically designed to behave inelastically by developing flexural plastic hinges at each end of the column, while the remainder of the bridge is to remain elastic. Thus, a bridge column adhering to ABC methods must also satisfy minimum seismic design codes. Several researchers have studied precast bridge column solutions: Kwan and Billington [2003a; 2003b] analyzed the use of unbonded posttensioning in a segmentally precast concrete bridge pier system; and Billington and Yoon [2004] investigated the use of fiber-reinforced cement-based composites at plastic hinge regions.

1.2 MOTIVATION FOR USING HYBRID FIBER-REINFORCED CONCRETE (HYFRC)

Because implementation of ABC requires revisions of a conventional bridge design, an opportunity exists to simultaneously improve other aspects of the bridge. Cracking in reinforced concrete bridges is of particular interest. During seismic loading, bending moments occur at the column's ends, resulting in flexural cracking and the spalling of concrete cover. Prior to such loading, corrosion products produced on the surface of embedded rebar may crack the concrete matrix surrounding it, potentially resulting in reduced lateral load carrying capacity. Thus, advancements to a more crack-resistant concrete composite would greatly increase structural durability.

Hybrid fiber-reinforced concrete (HyFRC) is considered a structurally advantageous alternative to plain concrete. Hybridization of fibers typically consists of polymer microfibers and hooked-end steel macrofibers of different lengths, and is necessary to achieve a performance-based design methodology known as Deterioration Reduction through Micro- and Macrocrack Control (DRMC) [Blunt and Ostertag, 2009b]. At the initiation of microcracking, microfibers begin to arrest and to bridge cracks as a first level of matrix reinforcement. With increasing stress, the microcracks eventually propagate into larger cracks, at which point macrofibers become most effective in resisting cracks. Unlike plain concrete, in which microfibers may coalesce into a few dominant cracks, when designed properly the multi-scale crack control provided in HyFRC results in numerous finer cracks. By controlling the cracking behavior of the concrete, toughness may be increased significantly over large deformations. The multi-scale approach is shown schematically in Figure 1.1.

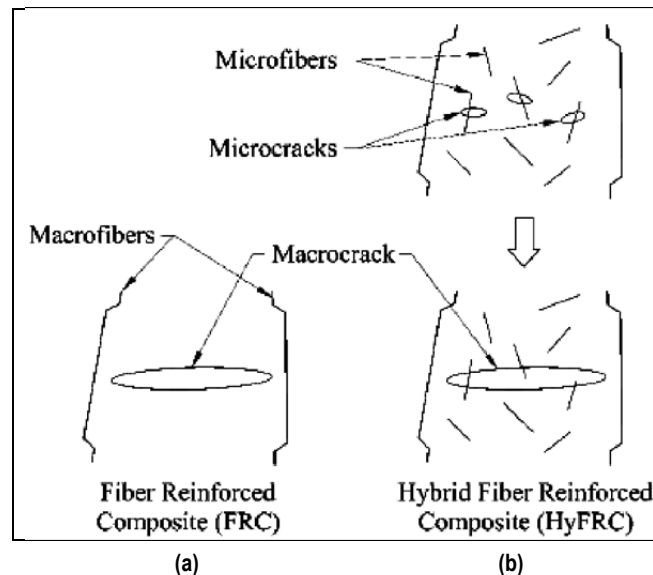


Figure 1.1 Schematic of crack-fiber interactions: (a) FRC with macrofibers only; and (b) HyFRC with micro- and macrofibers.

Deflection-hardening behavior can be achieved using HyFRC [Blunt and Ostertag 2009a], which is characterized by having a higher peak load than the matrix cracking load in specimens subjected to flexure. Such validation can occur through beam bending tests. When adhering to the DRMC methodology, the concrete is required to achieve a tensile strain equivalent to the design yield strain of the rebar (0.002). Because reinforced concrete (RC) bridge columns act as beam-columns during lateral loading, use of a deflection-hardening concrete may reduce cracking during a seismic event.

While the use of HyFRC is desirable in controlling cracks caused by applied loading, its advantages extend to durability enhancements not typically considered by structural designers. In particular, internal crack-inducing processes, such as reinforcement corrosion and alkali-silica reaction (ASR), may significantly reduce bridge longevity, resulting in continual rehabilitation or premature replacement. Ostertag and Blunt [2010] showed the corrosion current density in RC specimens composed of HyFRC was lower in comparison to plain concrete specimens after being subjected to the same load levels prior to corrosion experimentation. The HyFRC produced finer cracks when loaded, reducing saltwater ingress from the external environment. After the steel reinforcement's passive film has been destabilized due to chloride ions in the saltwater, corrosion product formation may begin. Fibers in the concrete were able to provide confinement to the product growth, thus limiting it [Grubb et al. 2007]. The confining mechanism of volumetrically expanding products is similar to ASR [Yi and Ostertag 2005]. Thus, the use of HyFRC produces composites that may improve durability from applied load and environmental reactions, two primary sources of damage that affect RC bridges.

1.3 HYFRC IN BRIDGE COLUMNS

Two experimental columns using HyFRC were fabricated and seismically tested by Panagiotou et al. [2014] Because the inclusion of fibers generally hinders the casting of concrete in heavily reinforced sections of structural elements, HyFRC with high workability and uniform self-compactability was developed specifically for cast-in-place construction. The developed concrete, known as self-consolidating HyFRC (SC-HyFRC), exhibited proper deflection-hardening behavior while attaining slump flow diameters in the range of 18 to 20 in.

The 1:4.5 scale columns both possessed a longitudinal steel ratio of 1.2% and a transverse volumetric steel ratio of 0.37%. Because of HyFRC's high ductility, the transverse ratio was designed at nearly half the value of a typical CalTrans bridge. The columns differed primarily in how inelastic behavior would be accommodated. The first column (Test Specimen 1, or TS-1) incorporated a rocking behavior by unbonding the longitudinal bars of the column near the columnbase interface. The second column (Test Specimen 2, or TS-2) was allowed to develop a flexural plastic hinge and utilized a corrugated steel duct pipe to mitigate cracking at the column base-foundation interface. In an effort to spread plasticity in the plastic hinge, this column also used stainless steel longitudinal bars. The SC-HyFRC columns performed well when subjected to static, uni-directional lateral loading, as damage due to spalled concrete was limited until drift ratios 3.6%. The axial load capacity of the column was maintained even to drift ratios up to 11.3%, which was the final tested drift cycle.

Trono et al. [2014] investigated a 1:3 scale rocking, post-tensioned HyFRC column subjected to dynamic seismic loading. The experimental column used several design details to reduce or eliminate residual deformations after seismic loading, including fully unbonded, post-

tensioned steel strands and precast HyFRC at the column base. While subjected to seven imposed ground motions on a tri-directional shake table, the column reached a peak drift of 8.0% and had a cumulative residual drift of under 0.4%, outperforming an experimental reference column that had a cumulative residual drift of 6.8%.

1.4 RESEARCH OBJECTIVES

The main research objectives of this project can be summarized as follows: (i) detailing and fabricating a bridge column consistent with both the ABC and DRMC methodologies; and (ii) designing a column so that its seismic performance meets or exceeds the mechanical properties of cast-in-place HyFRC columns of similar longitudinal reinforcement and gross dimensions.

For the purposes of expediting construction, a precast solution is investigated. First, a precast tube element was fabricated using a steel corrugated duct as the tube's inner surface and removable formwork as its outer surface. The tube contains the column's longitudinal and transverse reinforcement and is cast with HyFRC. To accommodate large lateral displacements, a rocking mechanism similar to that of the TS-1 specimen tested by Panagiotou et al. [2014] is utilized.

Use of a precast tube design offers several intended advantages over conventional cast-in-place operations. The benefits to be considered in this project include the following:

- ***Accelerated construction time:*** Utilizing the tube as a precast element eliminates the need for fabricating the column's steel rebar assembly at the construction site as the tube already contains the column's longitudinal and transverse reinforcement. Once the tube is installed into a foundation through typical cast-in-place methods, the tube also acts as permanent formwork for the casting of its hollow core.
- ***HyFRC limited to the column shell:*** Because the concrete nearest the surface of the column receives the highest stress and damage in a seismic event, the use of HyFRC as a shell layer is appropriate for its crack-controlling behavior. Additionally, the cost of the column may be reduced by not using fibers throughout the entire volume of the column.
- ***Higher quality control:*** The widespread use of fiber-reinforced concrete is currently limited. Because production of the tube, which is the only bridge component to contain fibers, is offsite, specially trained individuals are not required onsite during cast-in-place operations. In addition, fabricating the tube in a more controlled environment allows for optimally compacted HyFRC, which allows more even distribution of fibers within the concrete matrix. Higher than typical volumes of fibers, which normally reduce the concrete's cast-in-place workability, may also be tolerated due to ideal casting conditions.

The column, hereafter known as the *tube column*, is compared directly to the seismic performance of TS-1, as both columns utilize the same base rocking design, have the same longitudinal steel reinforcement ratio, and have the same external dimensions.

1.5 ORGANIZATION OF THE REPORT

The report is organized into five sections. The first section introduces the motivation and concept for using accelerated bridge construction with a HyFRC composite material. The second section describes the specimen design, structural materials used, and construction of the column. The third section provides information on the experimental test set-up, instrumentation used on the column, and loading protocol. The fourth section analyzes and discusses the observed and measured test responses acquired from the structural test. Included is a comparison between the performance of the tube column to cast-in-place columns of similar dimensions. The fifth and final section offers a summary and conclusions.

2 Specimen Design and Construction

2.1 DESIGN OF COLUMN

2.1.1 Details of Prototype Column

A number of bridge types in California were assessed in a study by Ketchum et al. [2004]. The column for this experiment based its design on a straight, cast-in-place, post-tensioned five-span box girder bridge. The longitudinal steel reinforcement ratio (ρ_l) was 1.2%, while the transverse steel reinforcement ratio (ρ_s) was 0.7%. The aspect ratio, defined as the ratio of the column height over the column diameter, was 8.3. Figure 2.1 shows additional design details of the bridge.

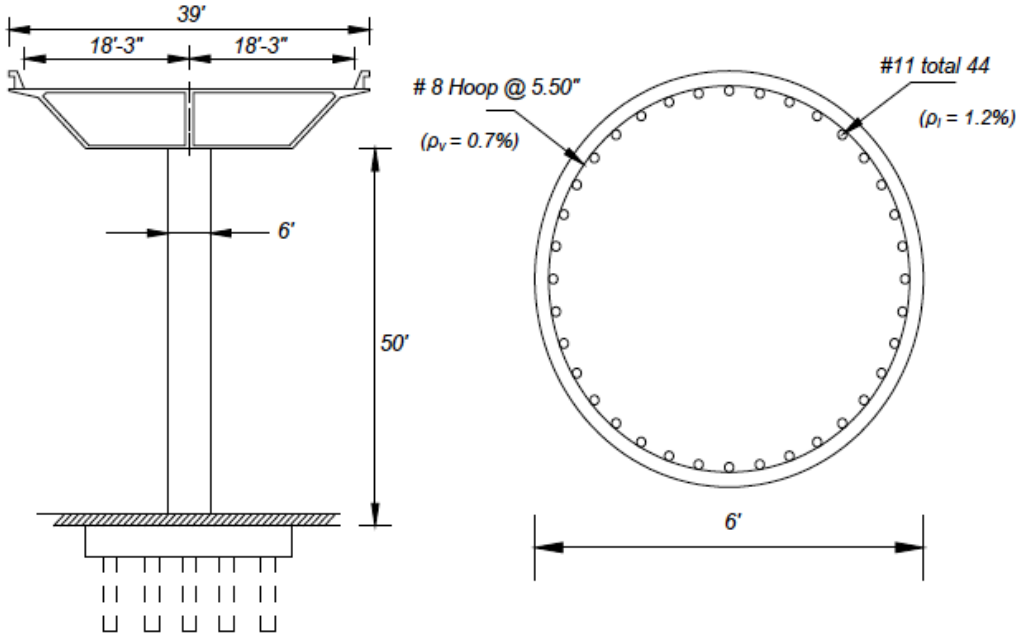


Figure 2.1 Elevation view and cross section of prototype bridge column [Ketchum et al. 2004].

2.1.2 Structural Details of Tube Column

To compare the structural performance of the tube column versus cast-in-place HyFRC bridge columns, its design was based on bridge columns tested by Panagiotou et al. [2014] Because the precast tube and its concrete core would not be monolithically cast with the column's foundation, a cold joint would be present at the column-foundation interface. To address this issue, a rocking design was chosen to accommodate large lateral displacements. Thus, Panagiotou et al.'s TS-1 specimen, which utilized a rocking design, was selected as the reference column for this project. In turn, the design of TS-1 was based on the prototype column by Ketchum et al. [2004]

Table 2.1 lists the external dimensions of the tube column, TS-1, and the prototype column; Figure 2.2 shows the structural details of the tube column. The diameter (D) was 16 in. for both the tube column and TS-1. The height (H), defined as the measurement from the base of the column to the elevation where the lateral load is applied during structural testing, was 65.00 in. for the tube column. These dimensions result in an aspect ratio of 4.06. Due to a variation in experimental set-up, the height of the tube column differed slightly from the height of TS-1 (67.25 in.). While the diameter of the tube column was scaled geometrically, the value of H is derived from matching a similar ratio of M / VH of the prototype column, where M and V are the bending moment and shear at the column ends, respectively. This scaling assumes the prototype column's ratio of M / VH is equivalent to 4 with a mid-height inflection point.

Fabrication of a precast tube was possible through the use of a spirally corrugated 16-gauge galvanized A92 steel duct pipe. Due to its corrugations, the pipe diameter varied from 10 to 11 in. The steel duct pipe would act as the inner formwork for the precast tube, as well as the outer formwork for the column core. As summarized in Table 2.2, the tube was to be cast with HyFRC, while its core was to be cast with plain, unreinforced concrete. Compared to a column of the same external dimensions cast entirely with HyFRC, the tube column design has approximately 43% less HyFRC by volume.

Table 2.1 Comparison of column gross dimensions.

Specimen	Scaling factor	D (in.)	H (in.)	H / D
Tube Column	4.5	16	65.00	4.06
TS-1	4.5	16	67.25	4.20
Prototype	1	72	600	8.33

Table 2.2 Comparison of column concrete type and steel reinforcement.

Specimen	Column concrete	Longitudinal reinforcement	ρ_l (%)	Transverse reinforcement	ρ_s (%)
Tube Column	HyFRC exterior shell; plain concrete interior core	(12) No. 4	1.2	W4.0 Spiral @ 1.25 in. O.C.	0.87
TS-1	SC-HyFRC	(12) No. 4	1.2	W3.5 Spiral @ 2.50 in. O.C.	0.37
Prototype	Plain concrete	(44) No. 11	1.2	No. 8 Hoop @ 5.50 in.O.C.	0.70

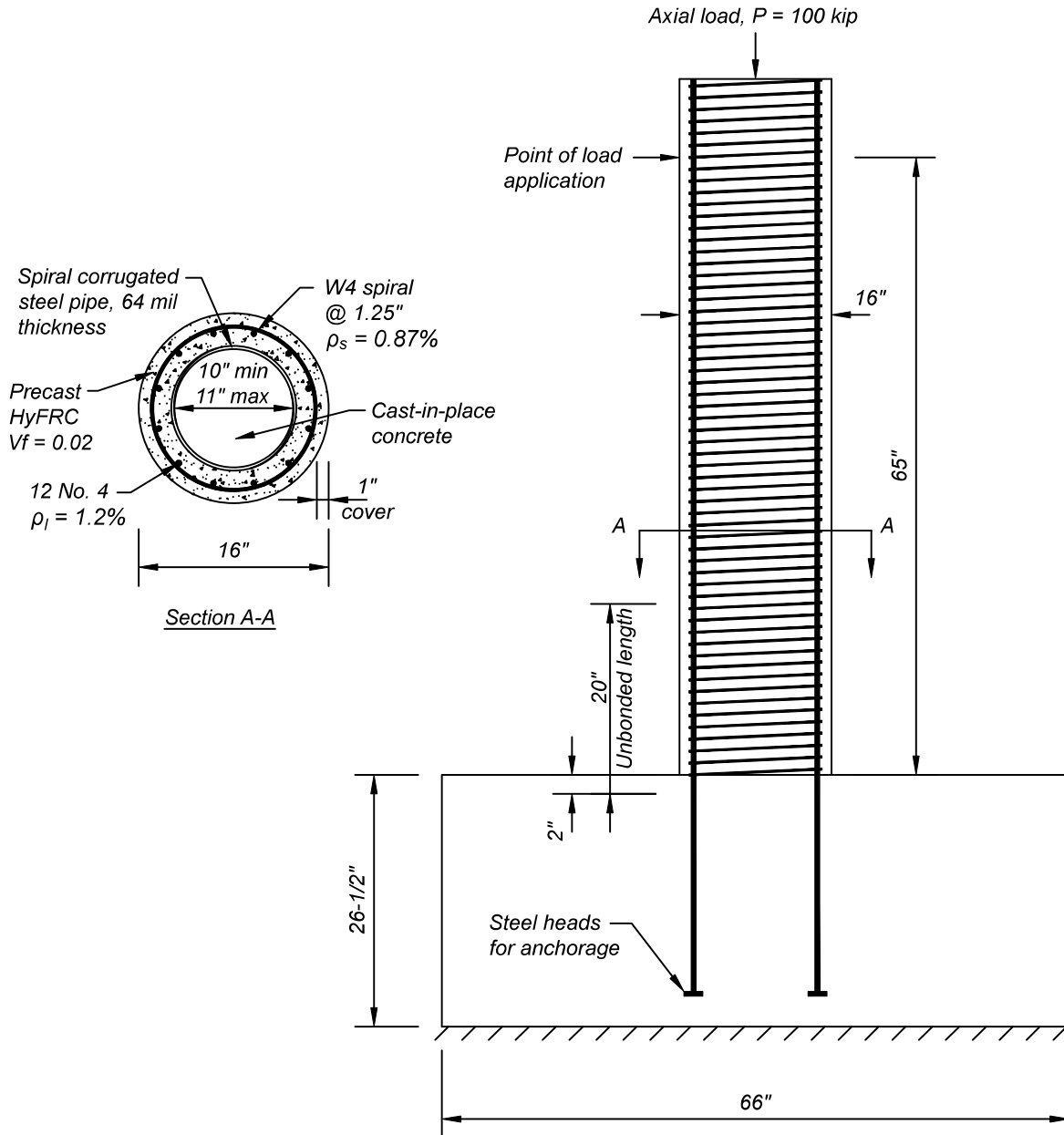


Figure 2.2 Tube column structural details. Steel pipe corrugations and foundation details not shown, for clarity.

To allow base rocking of the column, its twelve No. 4 A706 steel longitudinal bars were unbonded from the concrete for a total of 20 in.–18 in. in the lowest portion of the column, and 2 in. within the foundation. To unbond the bars, rubber mastic tape was first applied over the intended length to build up thickness between rebar ribs. By eliminating extrusions on the rebar, anchorage to the concrete provided by the ribs would be ineffective. Duct tape was then used as a final cover for further slippage and a protective layer during casting. At its termination within the foundation, the longitudinal rebar were capped with steel heads to provide anchorage during column lateral movement.

A continuous strand of W4.0 A82 galvanized steel wire was used as transverse spiral reinforcement. Spacing of the rungs was at 1.25 in. on center, resulting in a volumetric transverse steel reinforcement ratio (ρ_v) of 0.87%. This design ratio, which was nearly double the value for TS-1 (0.37%), was selected to increase the confinement effects of the column and delay longitudinal rebar buckling to high-drift ratio cycles. The transverse steel ratio was selected to be similar to that of the prototype column (0.70%).

2.2 MATERIALS USED IN CONSTRUCTION

2.2.1 Precast Tube HyFRC

2.2.1.1 Mix Design Proportioning

A concrete mix was developed specifically for the precast tube. The SC-HyFRC previously used for TS-1 was utilized as a baseline mix design. More details on the development of the baseline mixture may be found in Kumar et al. [2011]. Table 2.3 shows the SC-HyFRC concrete mix and the tube HyFRC concrete mix. Considering the tube's minimum thickness of 2.5 in. and the concrete clear cover of 1 in., limitations were imposed on the maximum size of batching materials to prevent potential congestion issues during casting. Coarse aggregates (3/8 in. maximum size) typically used in HyFRC were eliminated in the design of the mortar. However, the terms *concrete* and *HyFRC* will continue to be used when describing the tube structural cementitious composite.

The tube concrete was designed to adhere to the DRMC performance-based goals detailed by Blunt and Ostertag [2009b], resulting in a concrete that could exhibit deflection-hardening behavior and could reach a tensile strain matching the design yield strain of Grade 60 rebar. This behavior was achieved through the hybridization of different fiber types, as summarized in Table 2.4. Maintaining the same commercial fiber types as the baseline concrete mix, 0.315-in.-long polyvinyl alcohol (PVA) fibers and 1.18-in.-long hooked-end steel fibers were used for the tube concrete. Although a third fiber type, a 2.36-in.-long hooked-end steel fiber, is typically used, it was discarded due to the aforementioned concerns of material congestion during casting.

The fiber volume fraction (V_f) of the PVA fibers was set to 0.2% of total concrete volume, matching the baseline proportion. The steel fiber fraction was set to 1.8% of total volume, an increase over the baseline design of 1.3%. Because the strength of the tube concrete was expected to increase due to an absence of coarse aggregates, a higher fiber volume fraction was used to ensure proper deflection-hardening behavior. Samples tested from trial batches prior to casting of the tube column confirmed this behavior in beam bending. In addition, because the precast tube was intended to be cast within a laboratory or industrial environment where quality control would be optimized, a higher volume fraction of steel fibers could be accommodated without significant reductions in concrete compaction.

To have the concrete workable to flow through the tube opening, both a superplasticizer and viscosity modifying admixture (VMA) were used in the concrete design. The dosages of both were modified slightly from the baseline mix, since achieving a self-consolidating concrete was not a requirement for the tube. However, the final concrete had a slump flow diameter of 19 in., as shown in Figure 2.3, with workability appropriate for the casting method.

Table 2.3 Comparison of baseline and finalized saturated surface dry (SSD) proportions for tube HyFRC.

Material	SC-HyFRC for TS-1	HyFRC for Tube Column
	Weight for 1 yd ³ of concrete	Weight for 1 yd ³ of concrete
Cement Type I/II (lb)	670	825
Fly Ash Type F (lb)	220	275
Sand (lb)	1760	2201
Gravel (lb)	705	0
0.315 in. PVA Fiber (lb)	4.4	4.4
1.18 in. Steel Fiber (lb)	173	239
Batched Water (lb)	400	359
Superplasticizer (lb)	8.2	12.0
VMA (lb)	19.7	17.5
Fly Ash / Cementitious	0.25	0.25
Water / Cementitious	0.45	0.35
PVA Fiber Volume (%)	0.20	0.20
Steel Fiber Volume (%)	1.30	1.80
SP Wt-% Binder	0.93	1.09
VMA Wt-% Binder	2.21	1.59

Table 2.4 Fiber properties.

Fiber Type	Typical HyFRC V_f (%)	TS-1 V_f (%)	Tube Column V_f (%)	Length (in.)	Diameter (in.)	Aspect Ratio	Strength (ksi)	Elastic modulus (ksi)
PVA	0.2	0.2	0.2	0.315	0.0016	200	230	6090
Steel-1	0.5	1.3	1.8	1.18	0.0217	54.5	160	29000
Steel-2	0.8	0	0	2.36	0.0295	80	140	29000



Figure 2.3 Slump flow test of tube HyFRC.

2.2.1.2 Mechanical Properties

Laboratory test specimens were cast from the same batch of HyFRC used to produce the precast tube. Three 6 in. diameter \times 12 in. height compression cylinders were produced, as well as three 6 in. \times 6 in. by 24 in. long beams.

The compression test results shown in Table 2.5 and Figure 2.4 show the HyFRC used for the tube was relatively high-strength, achieving an average compressive strength of 9.55 ksi, with an average strain of 0.0042 at peak stress and an elastic modulus of 3650 ksi. Due to a low water-to-cementitious material ratio of 0.35, as well as an absence of coarse aggregate, a high compressive strength was expected.

Beams were tested in four-point bending per ASTM C1609 [2006], with results of the test shown in Table 2.6 and Figure 2.5. Deflection-hardening behavior can be seen in the plotted load-deflection curves for all considered specimens, as the peak loads of the beams are greater than the cracking load of the concrete matrix. Based on the load-based flexural performance goal methodology of Blunt and Ostertag [2009b], who used the same beam dimensions and test set-up, the minimum load to achieve the design tensile strain matching the value of Grade 60 rebar yielding was satisfied. Finally, the toughness of the beam is apparent by the gradual softening curve produced after the beams' peak load is achieved.

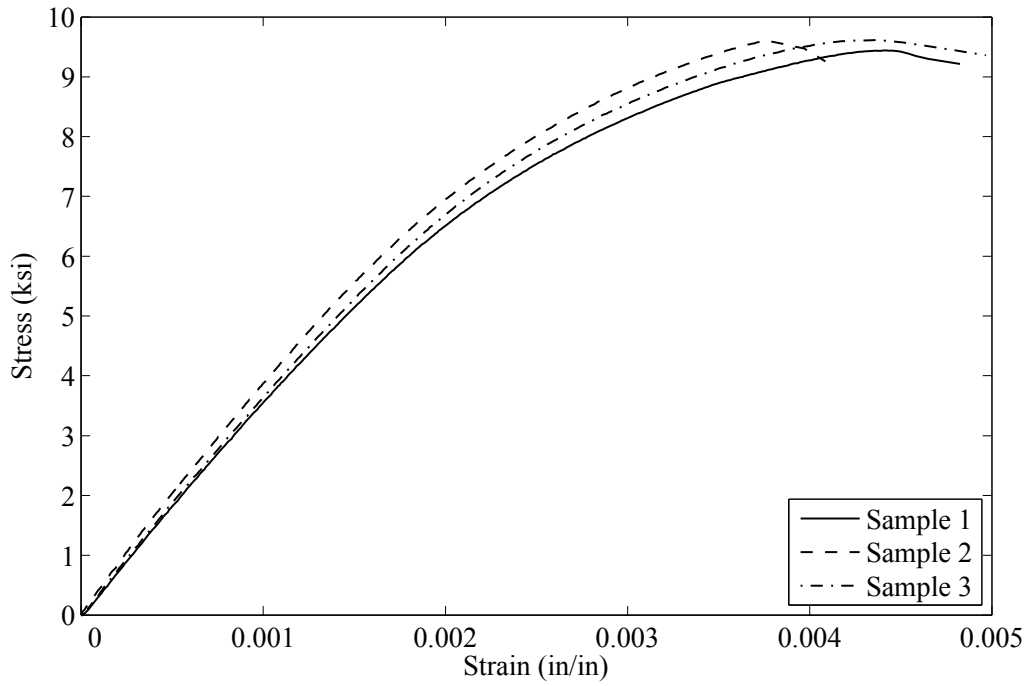


Figure 2.4 Tube HyFRC compression test results.

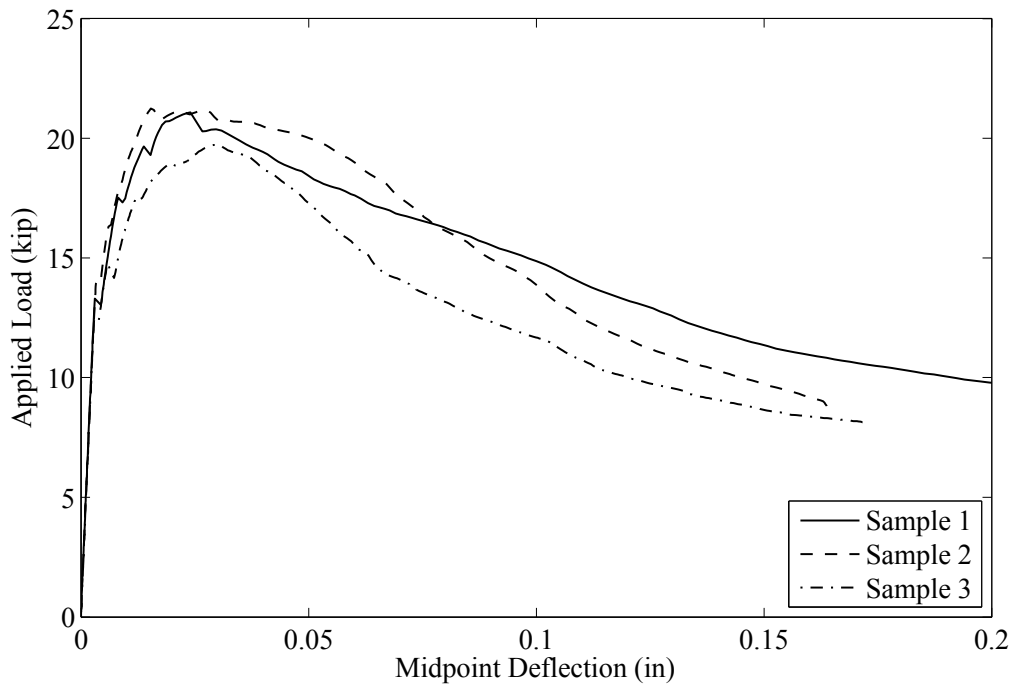


Figure 2.5 Tube HyFRC beam bending test results.

Table 2.5 Compression test results of tube HyFRC after 73 days.

	Sample 1	Sample 2	Sample 3	Average
f_c (ksi)	9.44	9.61	9.61	9.55
ϵ_0 (in./in.)	0.0044	0.0037	0.0044	0.0042

Table 2.6 Bending test results of tube HyFRC after 73 days.

	Sample 1	Sample 2	Sample 3	Average
P_{peak} (kips)	21.08	21.24	19.74	20.69
δ_{peak} (in.)	0.0240	0.0153	0.0299	0.0231
$P_{0.03}$ (kips)	20.38	20.89	19.74	20.34
% Peak	96.65	98.36	100.0	98.34
$P_{0.12}$ (kips)	13.31	11.62	10.02	11.65
% Peak	64.14	54.70	50.79	56.54
$T_{0.12}$ (kip-in.)	2.01	2.06	1.77	1.95

2.2.2 Core Concrete

The concrete for the core of the specimen was designed as a plain, normal-strength concrete to be batched in the laboratory. Using an existing mix design having a nominal 5 ksi compressive strength with a water–cement ratio of 0.48, the column core concrete was found to have a compressive strength of 6.35 ksi at an age of 46 days. Detailed mix proportions may be found in Appendix A.

2.2.3 Steel

Several types of steel were used in the column specimen, as summarized in Table 2.7. Column longitudinal and foundation reinforcement adhered to A706 Grade 60 steel. Twelve No. 4 longitudinal bars were used in the column. Transverse reinforcement consisted of a continuous spiral tied around the longitudinal bars. The spiral A82 galvanized steel had a gauge size of W4.0 (0.226 in. diameter) and was spaced vertically at 1.25 in. on center.

Table 2.7 Summary of steel used in specimen.

Type of steel	ASTM designation	Size / gauge
Longitudinal reinforcement	A706, Grade 60	No. 4
Transverse reinforcement	A82, galvanized	W4.0
Foundation reinforcement	A706, Grade 60	No. 3, No. 4
Corrugated pipe	A92, Galvanized	16 gauge

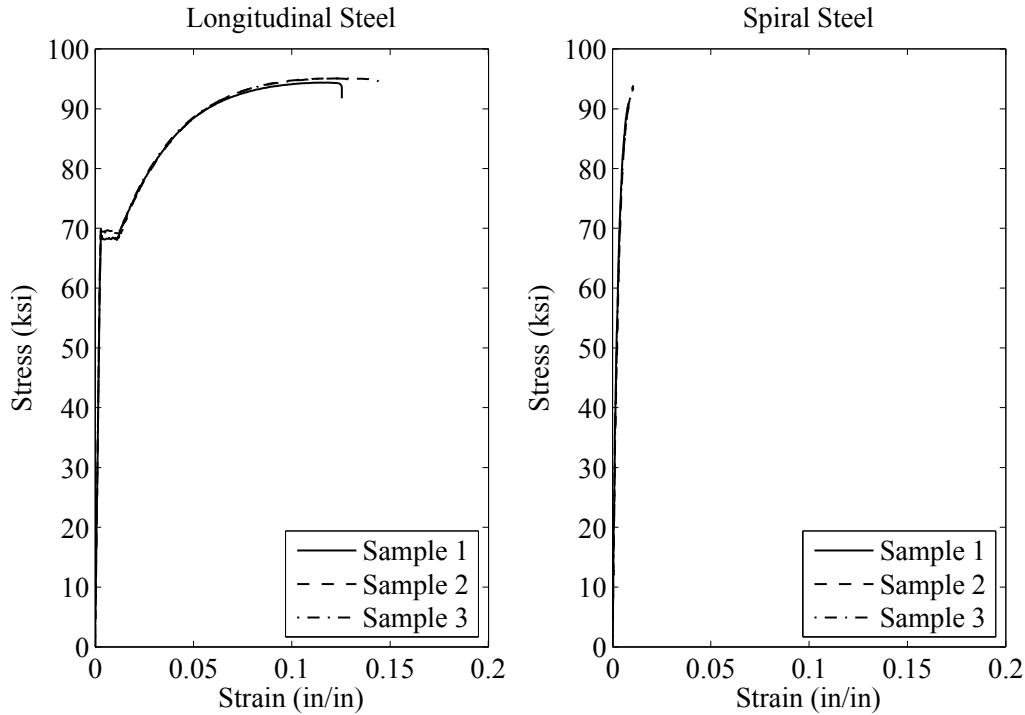


Figure 2.6 Steel reinforcement tensile test results: (a) longitudinal steel; and (b) spiral steel.

Based on tensile testing results, as shown in Figure 2.6, the longitudinal rebar exhibited a yield stress of approximately 69 ksi and an ultimate stress of approximately 95 ksi. The spiral reinforcement did not exhibit a yield plateau. Using the 0.2% offset method, the yield stress was approximately 78 ksi, while the ultimate stress was approximately 93 ksi.

The use of a 16-gauge (0.064 in.-thick) A92 galvanized steel corrugated pipe was necessary for providing an inner surface for the precast concrete tube. The spiral corrugations had a depth of 0.50 in., resulting in a pipe minimum and maximum diameter of 10 in. and 11 in., respectively.

2.3 CONSTRUCTION OF TEST SPECIMEN

2.3.1 Precast Tube

Construction and casting of the column specimen took place in the structural engineering laboratory of Davis Hall at the University of California, Berkeley. Before assembly of tube reinforcing steel began, strain gauges were first placed on the longitudinal rebar. In the intended unbonding region, the bars were wrapped in rubber mastic tape and then duct tape.

Figure 2.7 shows the platform created to accommodate the placement and maintain the design spacing of the longitudinal bars. The bars were placed vertically onto the platform, and were allowed to extrude 18 in. from the bottom cast surface for later installment into the foundation. The transverse spiral reinforcement was attached to the longitudinal bars by steel wire ties starting at the base of the column and working upwards.

After the spiral reinforcement assembly was completed, the corrugated steel pipe was placed vertically on the platform to provide the inner casting surface of the tube. A removable 16-in.-diameter column mold was used to produce the tube's outer surface. As shown in Figure 2.8b, 1-in.-long hardened cement paste spacers were used to promote proper alignment of vertical elements during casting.

A single HyFRC batch with a volumetric yield size of 0.33 cubic yards was used for casting the tube and supplementary testing cylinders and beams. The concrete was poured into the tube at its top opening. To ensure adequate compaction, form vibrators were placed near the lower portion of the column. Long tapping rods and stick vibrators were used to force concrete through the tube. Two hooked steel bars were embedded into the tube at the top surface to allow for later lifting and transport by overhead crane. The column mold was stripped from the tube after 14 days of curing, with the outer concrete surface showing no significant defects or voids, suggesting proper concrete consolidation during the casting.

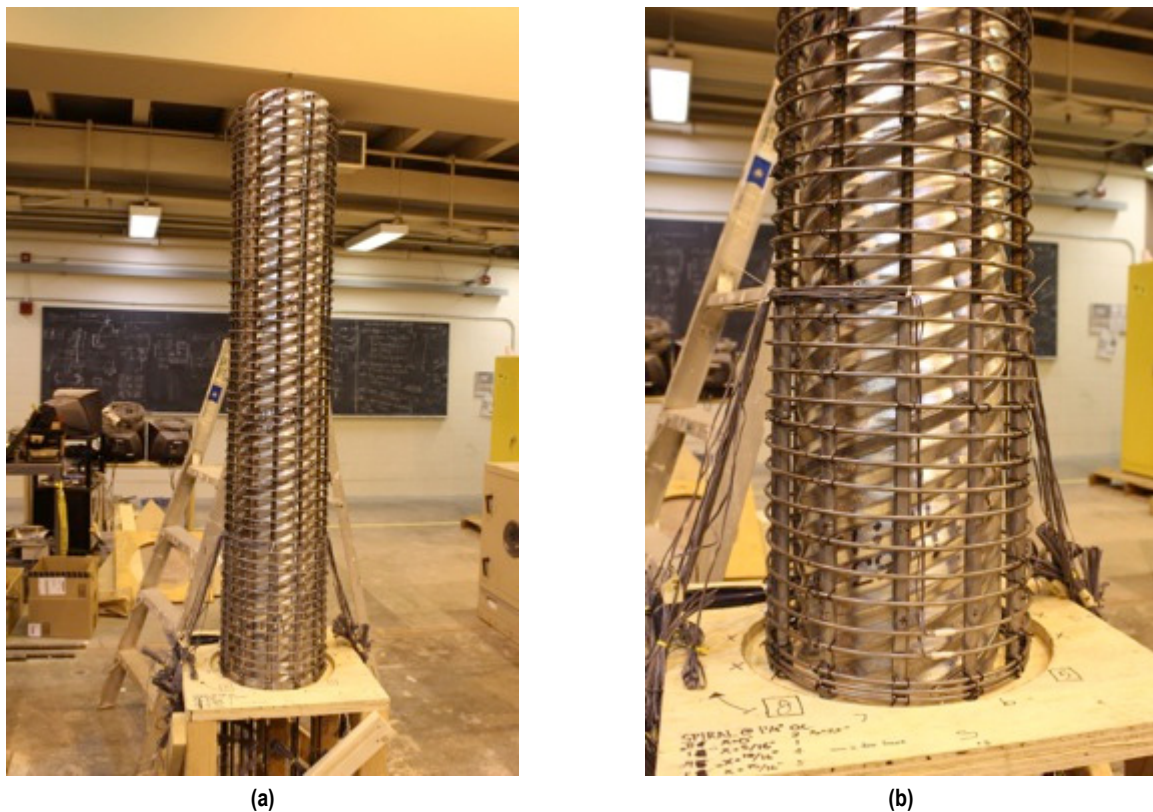


Figure 2.7 Elevation photographs of tube construction: (a) full elevation view; and (b) close up at unbonded region in tube.

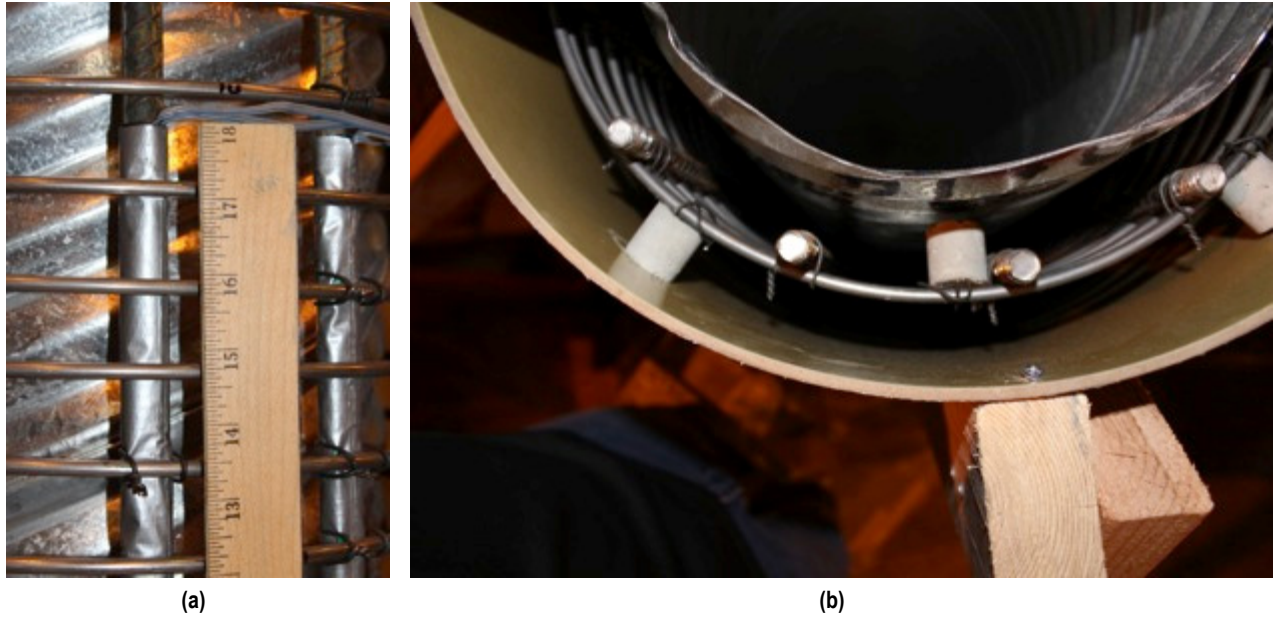


Figure 2.8 Detail photographs of tube construction: (a) unbonded rebar through use of duct tape within lower 18 in. of tube; and (b) plan view of tube cross section at top opening.

2.3.2 Foundation and Column Core

The next phase in construction required casting of the precast tube's extruded longitudinal bars within the foundation. A contractor assembled the foundation rebar cage and provided concrete through a mixing truck. Before casting, the precast tube was elevated on top of the foundation by the laboratory's crane such that the tube's extruded bars would be cast within the foundation and the bottom surface of the tube to coincide with casting of the upper surface of the foundation (Figure 2.9 and Figure 2.10).

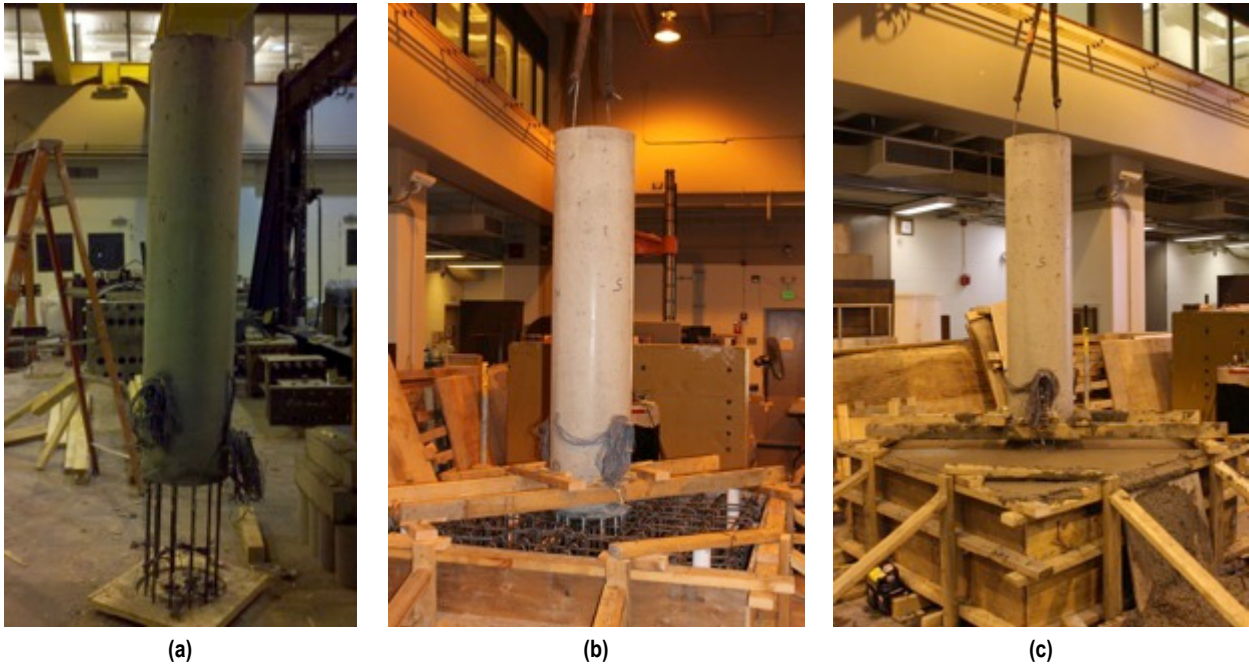


Figure 2.9 Elevation photographs of tube installment into foundation: (a) tube before installation; (b) tube aligned into foundation rebar cage; and (c) tube cast within foundation.

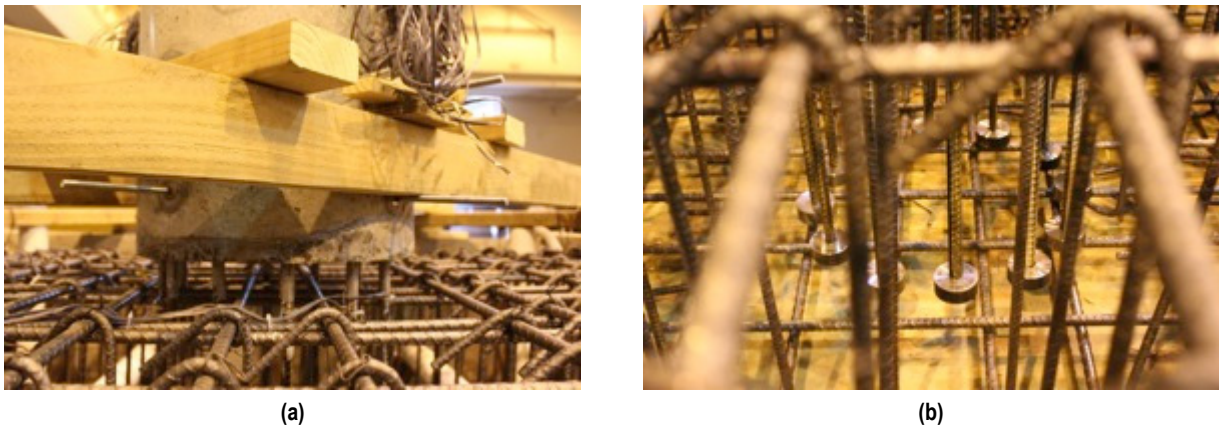


Figure 2.10 Detail photographs of tube installment into foundation: (a) close up at tube base, showing extruded longitudinal rebar from tube; and (b) extruded longitudinal rebar from tube within foundation rebar cage.



Figure 2.11 Top view of column prior to core casting.

After the foundation cured for 9 days, the hollow tube was filled with plain concrete. Figure 2.11 shows the column prior to core casting. A single concrete batch was again produced in the laboratory, though with a smaller yield size of 0.20 cubic yds. A stick vibrator was used to achieve compaction of the concrete. After the core was filled, four 1-in.-diameter steel rods were vertically embedded into, and extruded out from, the top surface of the column. This was to allow a steel spreader beam to anchor down onto the column during testing.

At the time of structural experimentation, the tube concrete was at an age of 67 days, the foundation concrete was at an age of 49 days, and the core concrete was at an age of 40 days.

3 Experimental Set-Up and Test Program

3.1 TEST SET-UP

Figure 3.1 shows the global test set-up of the column. A uni-directional cyclic loading protocol was selected to simulate seismic loading, with the lateral load applied through two horizontal actuators inclined at 45° to the direction of load, as shown in Figure 3.2. A gravity load of 100 kips was applied to the column through a built-up steel spreader beam, which had a vertical actuator at each end of the beam. Lateral loading was selected to occur in the East-West direction, with lateral displacement in each cycle initiating towards the eastern direction first.



Figure 3.1 Global view photograph of test set-up.



Figure 3.2 Detail photograph of horizontal actuators.

3.2 DATA INSTRUMENTATION

Of the twelve longitudinal rebar in the column, the four most eastern and four most western bars were fitted with strain gauges, for a total of eight bars (Figure 3.3). On each of these rebar, two gauges were positioned within the unbonded length of the rebar, while one gauge was embedded in the concrete foundation. Specifically, gauges were positioned 8 in. above, 4 in. above, and 4 in. below the column-foundation interface, for a total of three gauges. In addition, the spiral reinforcement near the base of the column also received internal instrumentation. Spiral rungs positioned approximately 1.25 in. and 2.50 in. above the column base on the North, South, West, and East faces of the column each had a strain gauge applied to it, resulting in eight total spiral strain gauges.

Vertical displacement transducers were used for external measurements. A set of four transducers was placed in series on both the western and eastern column faces, while two transducers in series were used on the northern and southern faces. Figure 3.4 and Figure 3.5 show the locations of the transducers. Typical transducer set-up is also shown in Figure 3.6. All transducers were positioned at elevations within the unbonded region of the column.

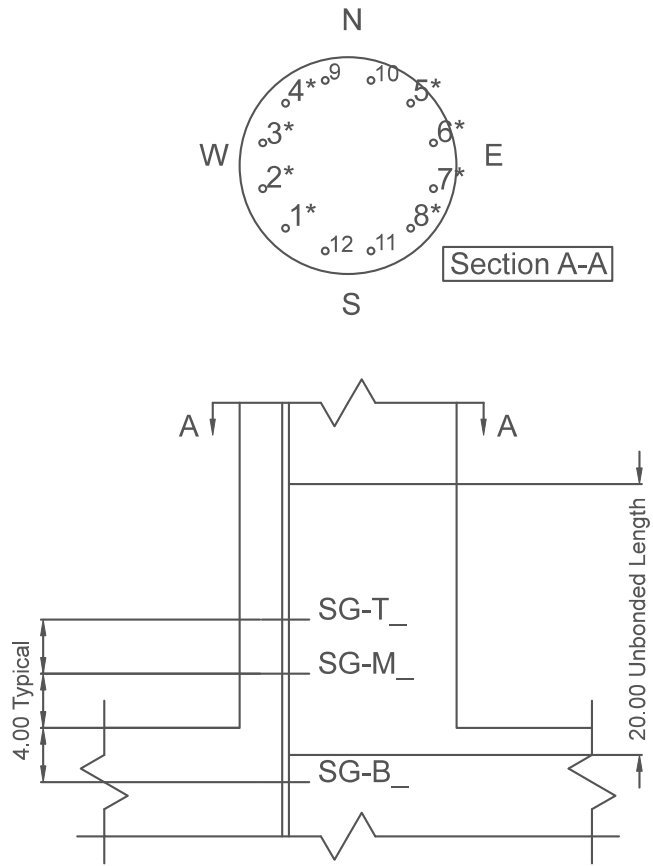


Figure 3.3 Location of strain gauges on longitudinal rebar. Section A-A shows rebar designation. (*) refers to rebar with strain gauges. Elevation view shows 1 rebar for clarity; units in inches.

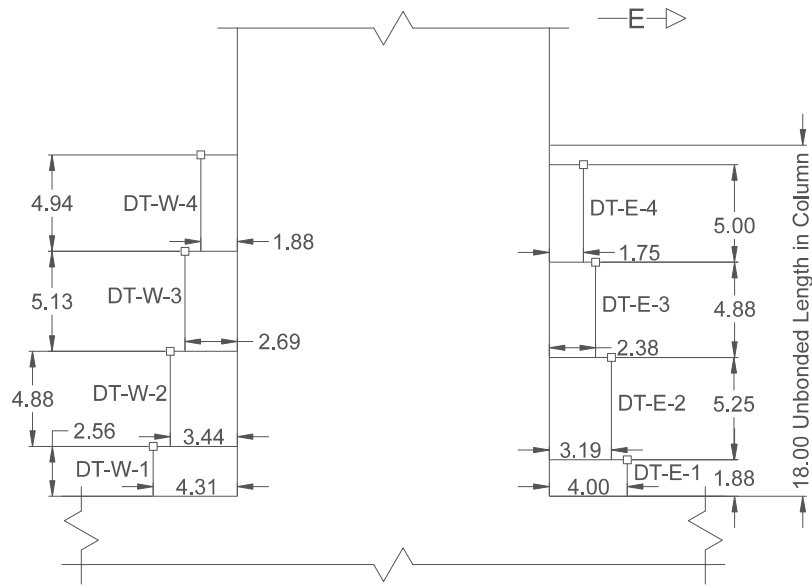


Figure 3.4 Locations of West and East face displacement transducers; units in inches.

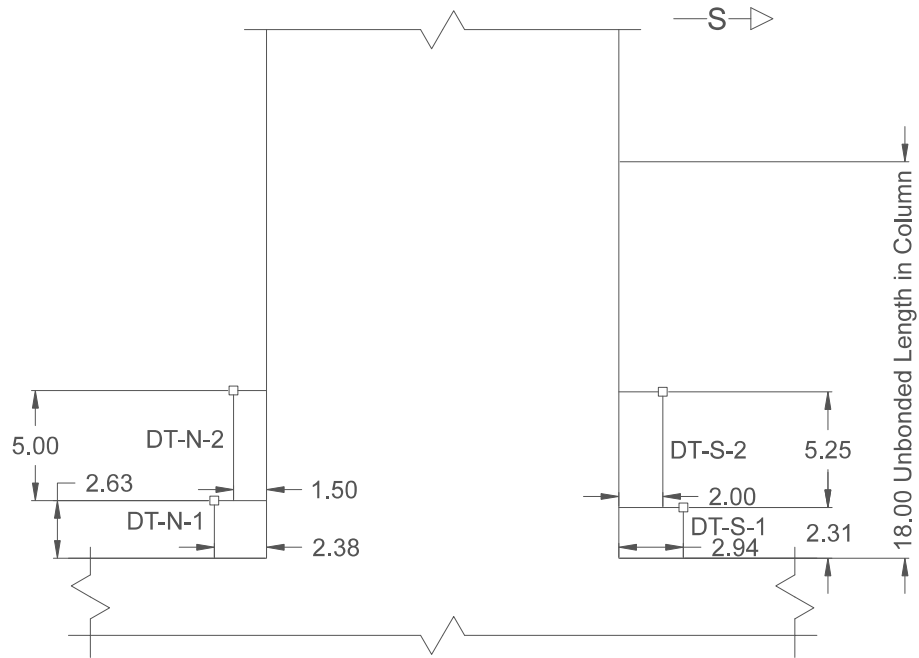


Figure 3.5 Locations of north and south face displacement transducers; units in inches.



(a)



(b)

Figure 3.6 Detail photographs of displacement transducers: (a) East column face; and (b) North column face.

3.3 LOADING PROTOCOL

The loading protocol of the column consisted of cyclically loading the column at predetermined target drift ratios. The drift ratio θ_r is defined as $\theta_r = \Delta / H$, where Δ is the applied lateral displacement applied at a height H (65.00 in.) above the foundation surface. The column was initially cycled three consecutive instances at the same drift ratio level before reaching the next series of cycles. At drift ratios of 4.20% and higher, the cycling was reduced to one instance. Although the loading protocol was similar to that of TS-1, the tube column was allowed to achieve a higher final target test drift ratio of 13.1% compared to the 11.3% maximum drift ratio achieved by TS-1. Figure 3.7 shows the lateral displacement history as a function of data steps.

As noted in Table 3.1, the actual applied drift ratios did not correspond exactly with target drift ratios. During progression of the test, eastward lateral displacement (corresponding to positive drift ratios) tended to be less than targeted, while westward lateral displacement (corresponding to negative drift ratios) tended to be more than targeted.

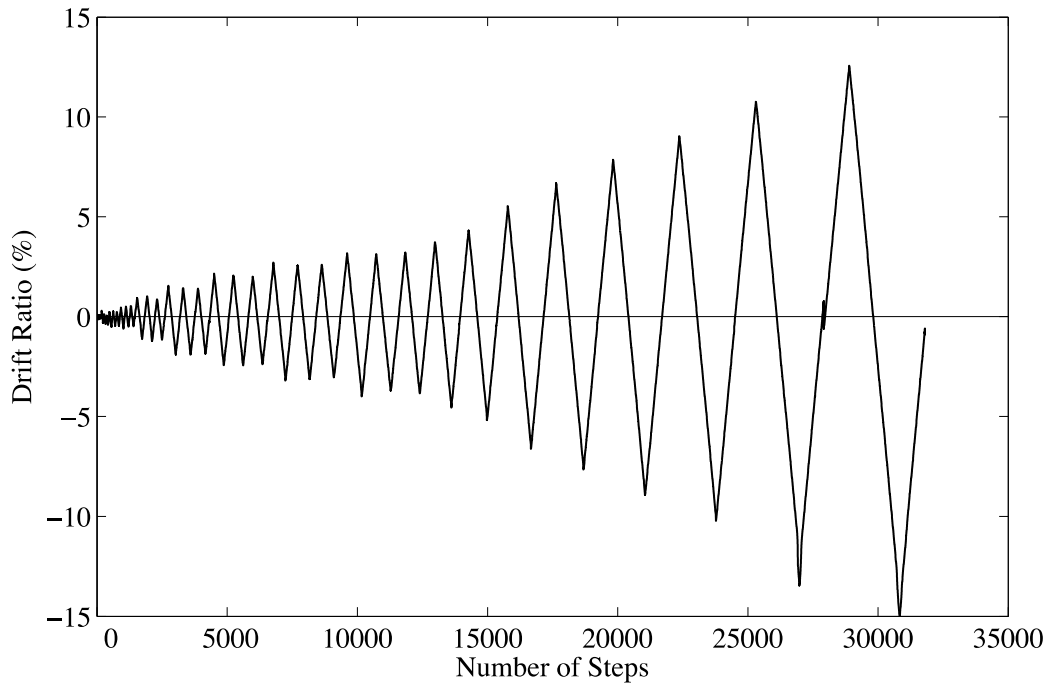


Figure 3.7 Actual lateral drift ratios applied.

Table 3.1 Number of cycles at target drift ratios ($H = 65.00$ in.).

Target drift ratio, θ_r (%)	Actual maximum drift ratio in cycle set (%)	Actual minimum drift ratio in cycle set (%)	Target displacement, Δ (in.)	Number of cycles
0.15	0.09	-0.14	0.10	3
0.30	0.30	-0.40	0.20	3
0.44	0.27	-0.51	0.29	3
0.60	0.53	-0.61	0.39	3
1.20	1.0	-1.2	0.78	3
1.80	1.6	-1.9	1.17	3
2.40	2.2	-2.4	1.56	3
3.00	2.7	-3.2	1.95	3
3.60	3.2	-4.0	2.34	3
4.20	3.7	-4.6	2.73	1
4.80	4.3	-5.2	3.12	1
6.00	5.5	-6.6	3.90	1
7.10	6.7	-7.7	4.62	1
8.30	7.9	-8.9	5.40	1
9.50	9.0	-10.2	6.18	1
11.3	10.8	-13.5	7.35	1
13.1	12.6	-15.1	8.52	1

4 Experimental Results and Discussion

4.1 LATERAL FORCE-DISPLACEMENT RESPONSE

The complete lateral load-drift ratio hysteretic response of the column is presented in Figure 4.1. A loss of stiffness in the column occurs at drift ratios larger than 1.2%, which may be more easily observed in Figure 4.2, which plots the hysteretic response up to drifts of 4.8%. Hardening behavior is observed past these drift ratios and continues until the column reaches the loading cycle corresponding to a drift ratio of approximately 4.8%. Two major load drops can be seen at higher drift ratios, corresponding to longitudinal rebar fracture. The first fracture occurred during the drift ratio step of 11.3% on westward loading, while the second fracture took place during the final drift ratio step of 13.1% on eastward loading. Fracture sounds could be heard during the mentioned drifts, likely corresponding to longitudinal rebar failure as well as spiral reinforcement failure.

Based on the response, the column shows considerable toughness, maintaining at least 88% of its maximum lateral load capacity at each load cycle up to drift ratios of 10%. In addition, the axial load capacity of the specimen did not significantly decrease during the entirety of the test.

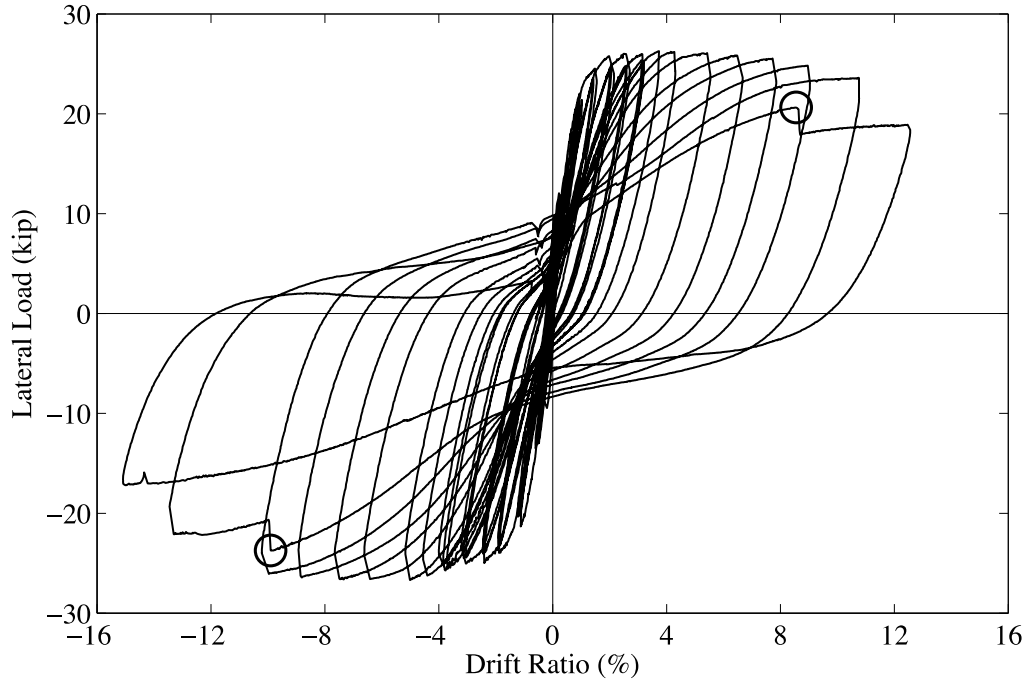


Figure 4.1 Complete lateral load-drift ratio response. Circle markers indicate points of longitudinal rebar fracture.

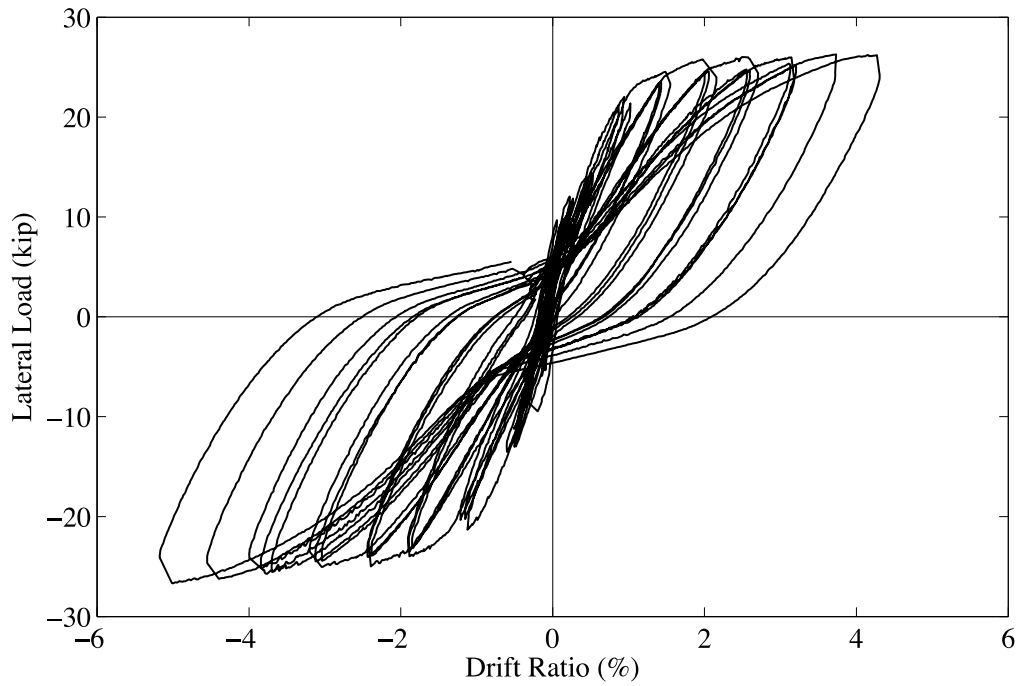


Figure 4.2 Lateral load-drift ratio response to $\theta_r = 4.8\%$.

4.2 ROCKING BEHAVIOR

Because of the tube column's rocking design, flexural cracks were not anticipated in the column's unbonded region, which encompassed the lowest 18 in. of the column. Figure 4.3 and Figure 4.4 show surface crack progression on the northeastern and western faces of the column, respectively. Cracks were observed starting at drifts of 0.60% and located 19–26 in. above the column base, just above the unbonded region. Subsequent loading cycles reveal flexural cracks present as high as 48 in. above the column base ($\theta_r=2.40\%$), while not being observed at elevations less than 19 in. (Figure 4.5). There was little change in flexural damage above the unbonded region to the column past a drift of approximately 2.4%, as shown by the lack of surface crack development in the sequence of photographs. While the rocking mechanism is attributed to the lack of cracking at the column base, HyFRC may have been effective in mitigating damage outside of the unbonded region. For instance, cracks on the tensile face of the column during the 3.6% drift cycle were observed to have a maximum width of approximately 0.016 in. Upon return to neutral position, opened cracks were seen closing to hairline widths.

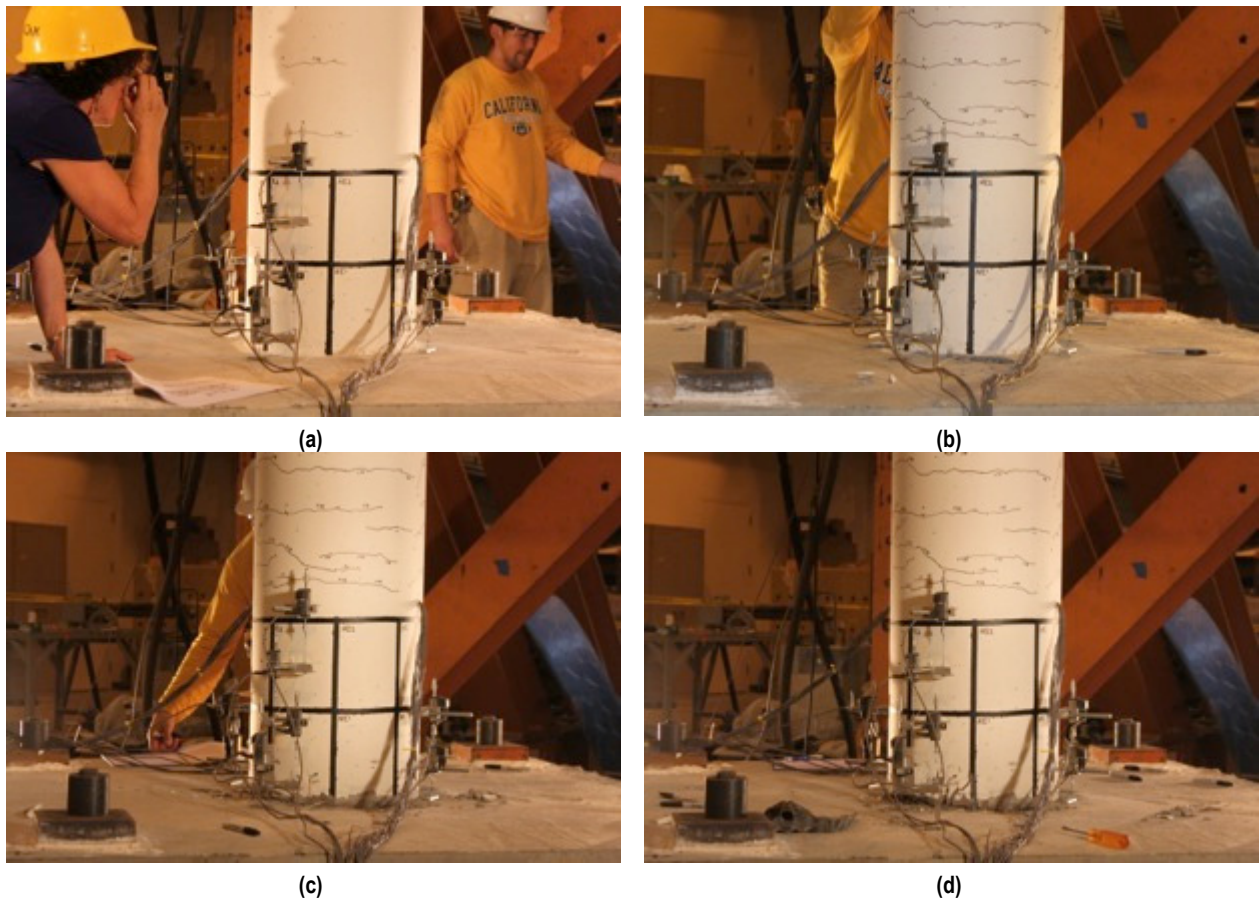


Figure 4.3 Northeast face of column at neutral position: (a) $\theta_r=0.60\%$; (b) $\theta_r=2.4\%$; (c) $\theta_r=6.0\%$; and (d) $\theta_r=11.3\%$.

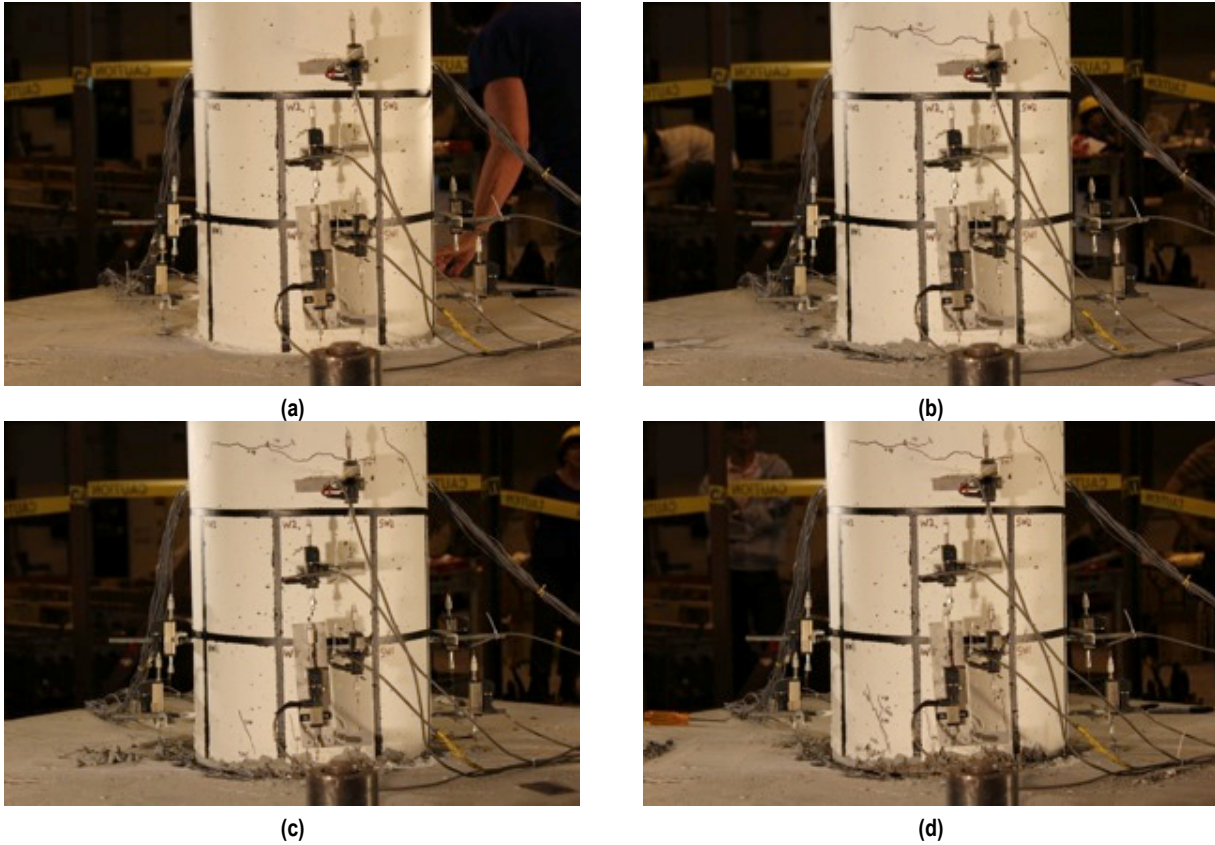


Figure 4.4 West face of column at neutral position: (a) $\theta_r=0.60\%$; (b) $\theta_r=2.4\%$; (c) $\theta_r=6.0\%$; and (d) $\theta_r=11.3\%$.



Figure 4.5 Elevation view of column: (a) West face in extreme tension, $\theta_r=2.4\%$; and (b) East face in neutral position, $\theta_r=2.4\%$.

During the test, the column exhibited seemingly rigid behavior, as shown in Figure 4.6. The figure shows a global view of the specimen subjected to maximum eastward displacement during the 11.3% drift cycle. The rocking behavior of the column may be quantified with the use of displacement transducer measurements. Figure 4.7 shows the measurements taken by the displacement transducers lowest in column elevation on the western and eastern faces of the column (DT-W-1 and DT-E-1, respectively). The nearly bilinear curve for each transducer suggests rigid rocking behavior in the West-East direction, with the change in slope caused by a neutral axis that does not pass through the center of the column. Figure 4.8 provides a plot of calculated column base rotation versus drift ratio up to a drift of 8.3%. The base rotation, θ_b , is calculated as $\theta_b = \frac{(DT_{W1}) - (DT_{E1})}{d}$, where DT_{W1} and DT_{E1} are the displacement transducer measurements at the W-1 and E-1 positions, respectively, and d is the horizontal distance between the points of measurements. As indicated in the curve's linearity, the relationship between the drift ratio and calculated base rotation is nearly equivalent. This again suggests the presence of the intended rocking behavior in the specimen, as the column acts nearly rigidly.



Figure 4.6 Column during extreme eastern drift, at $\theta_r=11.3\%$: (a) global view, viewing from southern side; and (b) close-up at western face, viewing from northern side, showing exposed longitudinal rebar.

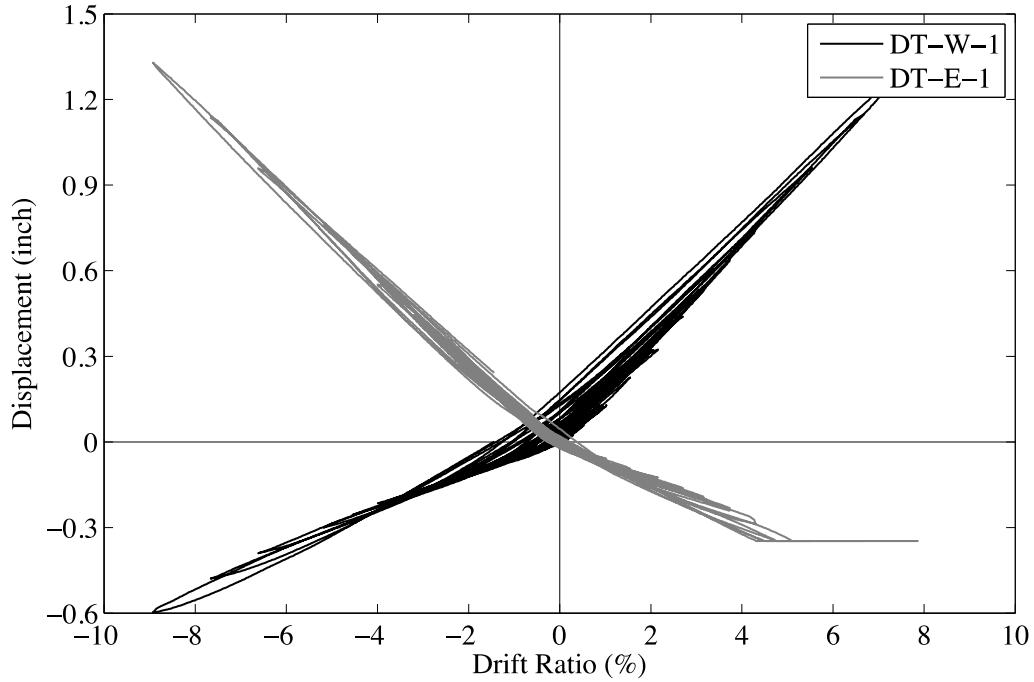


Figure 4.7 Displacement versus drift ratio based on column base displacement transducer measurements from DT-W-1 and DT-E-1.

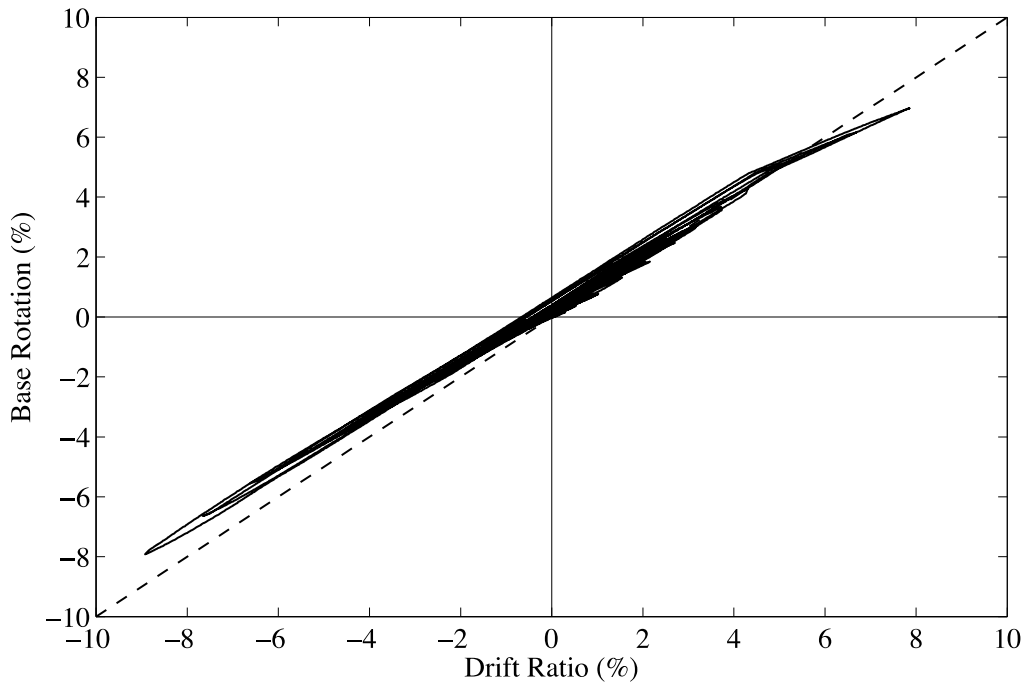


Figure 4.8 Column base rotation versus drift ratio, based on column base displacement measurements from DT-W-1 and DT-E-1. The dashed diagonal line represents perfectly rigid column movement.

Strain gauge measurements from the most extremely loaded longitudinal steel, namely bars 2, 3, 6, and 7, are presented in Figure 4.9 as a function of data steps. Strain gauges placed at an elevation 4 in. and 8 in. above the foundation base are denoted as “SG-M_” (Middle) and “SG-T_” (Top), respectively.

It was expected that the strains at the middle and top positions of the bar would be similar in magnitude due to its unbonding from the concrete. Bar 2 shows good correlation between both its strain gauges in this region. Bar 3 shows the peak positive strains of each load cycle having similar values, although the peak minimum strains do not coincide at the middle and later portions of the test. The strain gauge at the top position may have degraded, as indicated by its lack of smooth cyclic behavior at its minima. Bar 7 shows some correlation between its maxima and minima at certain durations of the test.

Because of the longitudinal bars’ plastic deformation, a residual vertical displacement was produced between the column base and foundation surface, as shown in Figure 4.10. The permanent uplift was measured by displacement transducers at the base of the column; see Figure 4.11.

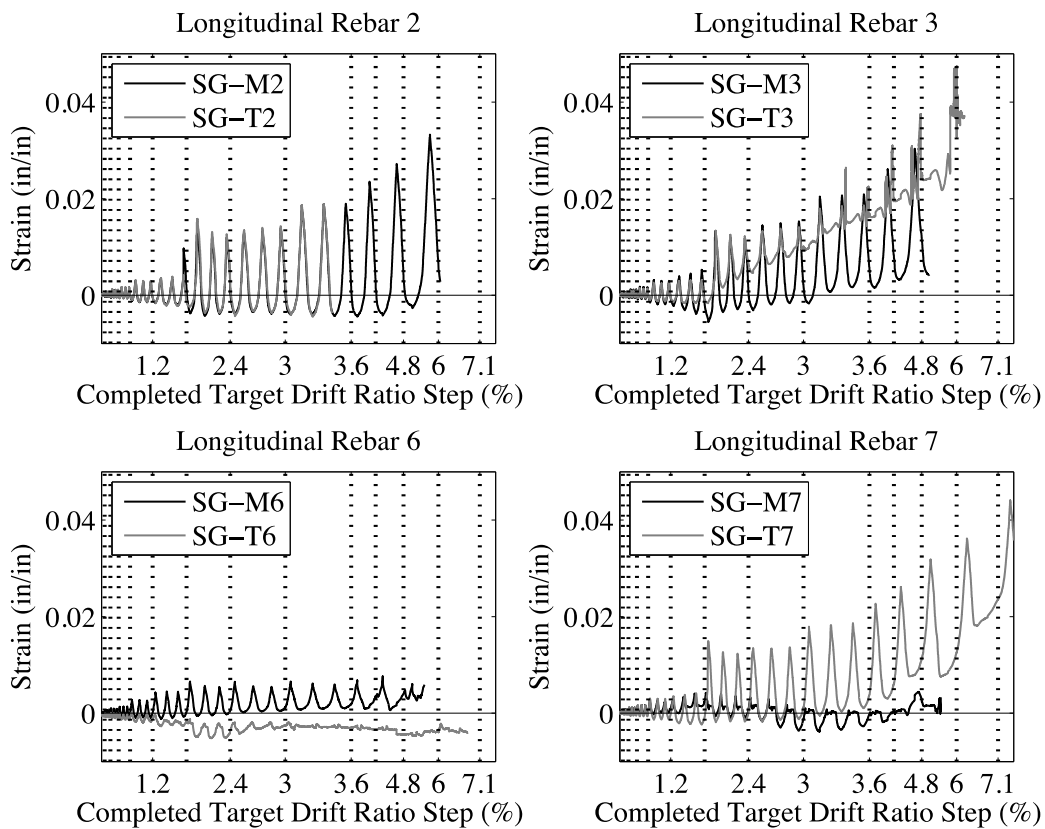


Figure 4.9 Strain gauge measurements as a function of data steps at the middle and top positions for longitudinal rebar 2, 3, 6, and 7. Vertical line intervals indicate the completion of a target drift ratio cyclic sequence.



Figure 4.10 East face of column at neutral position, $\theta_r=8.3\%$. Permanent vertical displacement can be observed between the column–foundation interface.

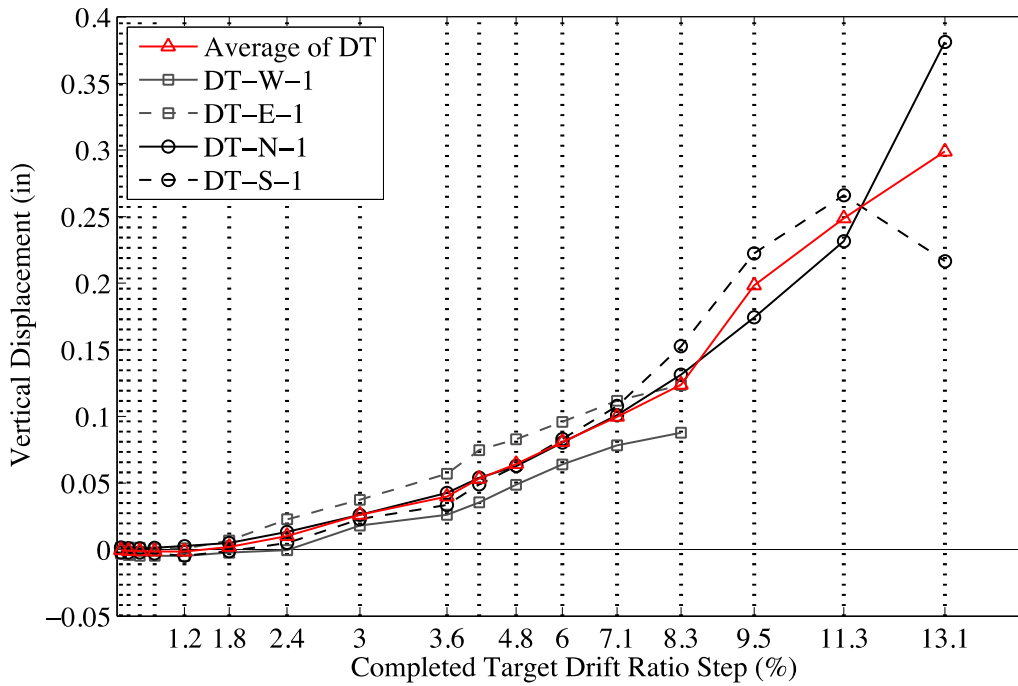


Figure 4.11 Residual vertical displacements.

4.3 COMPRESSION DAMAGE

Despite being subjected to drifts levels of over 10%, the column did not show spalling of concrete, as a physical loss of cover from the column was not observed. Compression damage was generally limited to splitting cracks formed at the base of the column, with the eastern face of the column exhibiting more damage than the western face. Figure 4.12 shows the progression of damage near the eastern column face, highlighted by a splitting crack near the SE1 and E1 grid boundaries. Smaller splitting cracks were observed on the western column face, as shown in Figure 4.13.

Plotted in Figure 4.14, strain gauge measurements were collected from the spiral transverse reinforcement on the western and eastern faces of the column at approximately 1.25 in. and 2.50 in. above the column base. Strain magnitudes were relatively low up to the 7.1% drift cycle, after which the strains generally increased during the later stages of the test. Additionally, during the 11.3% and 13.1% drift cycles, several noises were heard during the test, which was likely the result of spiral fractures. Fracture of the spiral steel may explain the non-cyclic measurements observed in some of the strain gauges.

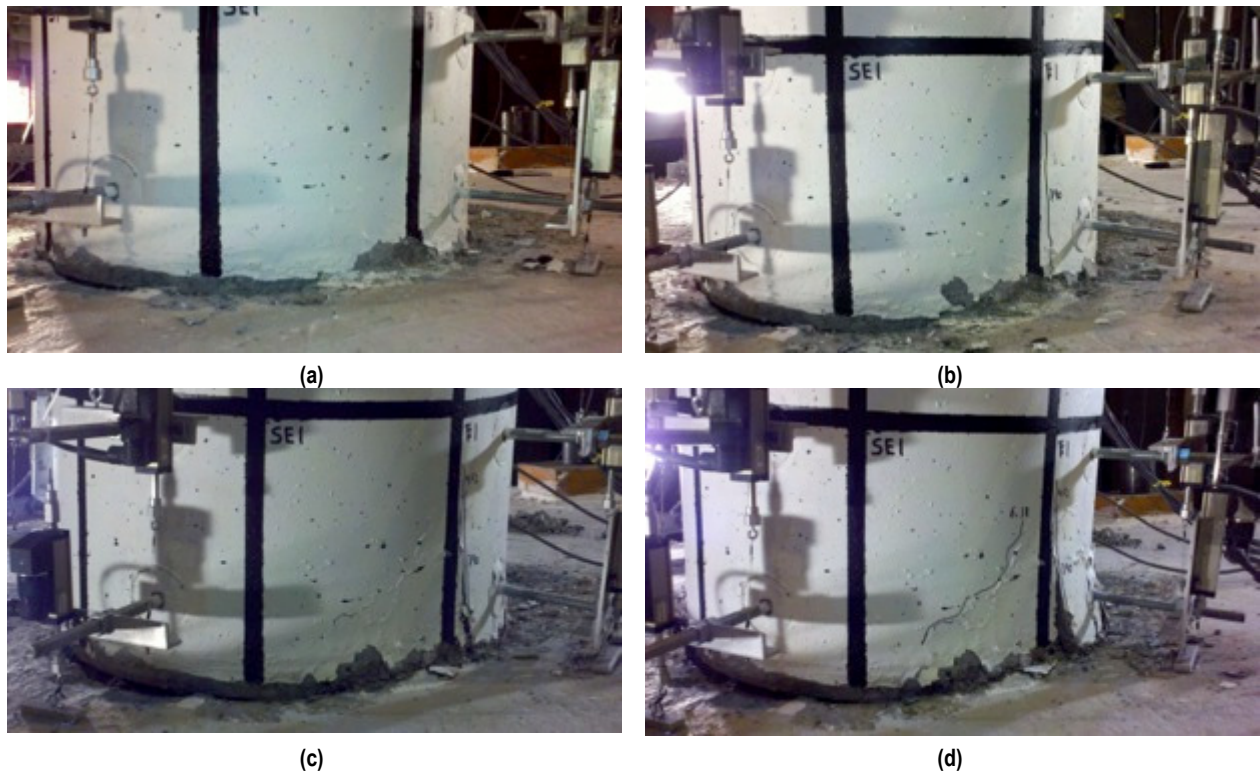


Figure 4.12 Southeast face of column at extreme eastward loading: (a) $\theta_r=4.8\%$; (b) $\theta_r=6.0\%$; (c) $\theta_r=9.5\%$; and (d) $\theta_r=11.1\%$.



Figure 4.13 Northwest face of column at extreme westward loading: (a) $\theta_r=8.3\%$; and (b) $\theta_r=9.5\%$.

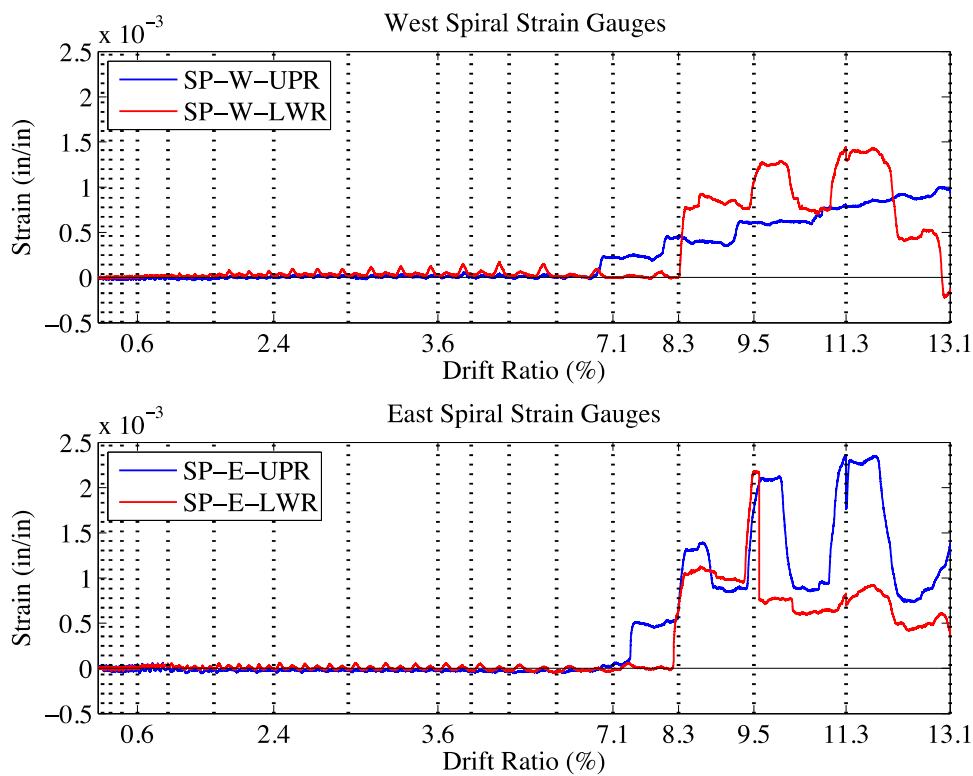


Figure 4.14 West spiral and East spiral strain gauge measurements.

Displacement transducers located at the western and eastern faces of the column provide some measure of compressive strains in the concrete. Measurements taken from the transducers were calculated into column surface smeared strains, with transducers nearest the foundation not considered due to the large displacements caused by base rocking. Figure 4.15 shows the strain profile of the column at extreme compressive loading. Compressive strains in the lowest elevations of the column reached approximately 0.0040 by the 6.0% drift cycle, nearly matching the strain at peak compressive strength of the HyFRC (0.0042). However, as mentioned earlier, the concrete surface damage consisted of splitting cracks, suggesting HyFRC's tendency to minimize cover spalling.

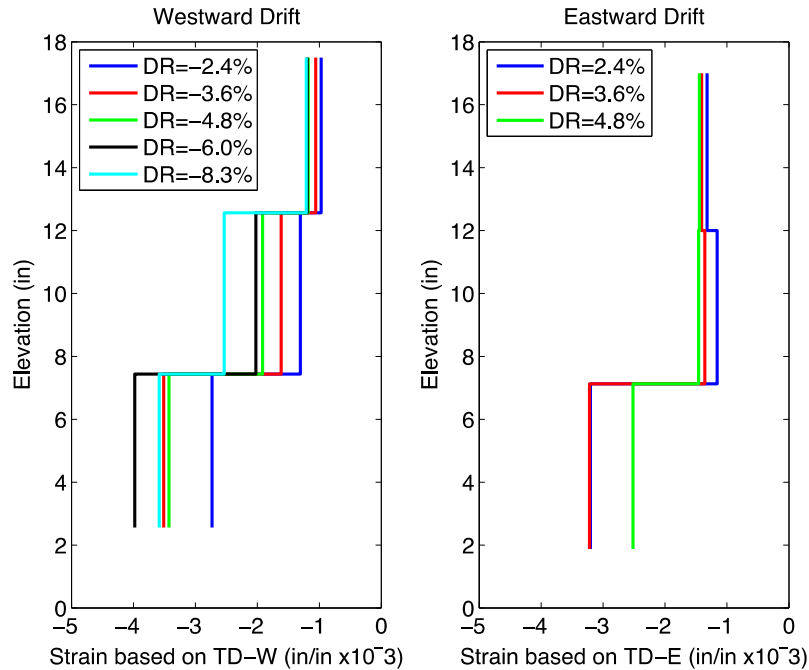


Figure 4.15 Extreme compressive strain profile based on displacement transducer measurements.

4.4 COMPARISON TO CAST-IN-PLACE COLUMNS

The specimen TS-1 provides a suitable comparison for gauging the tube column's structural performance. To summarize, the concrete of TS-1 consisted entirely of HyFRC while the tube column had a dual-phase design consisting of a HyFRC outer tube and plain concrete interior core. The longitudinal reinforcing details of the two columns were similar, with both having a 1.2% steel reinforcing ratio consisting of 12 No. 4 longitudinal bars. The transverse reinforcing ratio of TS-1 was 0.37%, which was less than half that of the tube column's transverse reinforcing ratio (0.87%). To accommodate large drift ratios, both columns employed a rocking mechanism at the column base by unbonding the longitudinal bars from the concrete in the lowest elevations of the column.

The complete lateral load-drift ratio hysteric response for the two columns is shown in Figure 4.16, while the response up to a target drift ratio of 5% is shown in Figure 4.17. Note the loading protocol of TS-1 halted at a maximum target drift ratio of 11.3%, while the tube column was allowed to achieve a target drift ratio of 13.1%.

Figure 4.18 again shows the hysteric response of the columns for the full test, but with the envelope curve highlighted for clarity. At drift ratios under 5%, the responses of both columns are similar. For westward movement (negative drift ratios), the curves of TS-1 and the tube column nearly overlap. A 3.4% difference in load is observed at a drift ratio of -4.4%. For eastward movement (positive drift ratios), a difference in magnitude of load is greater, although the curves generally suggest similar behavior. At a drift ratio of 4.2%, a load difference of 8.3% exists.

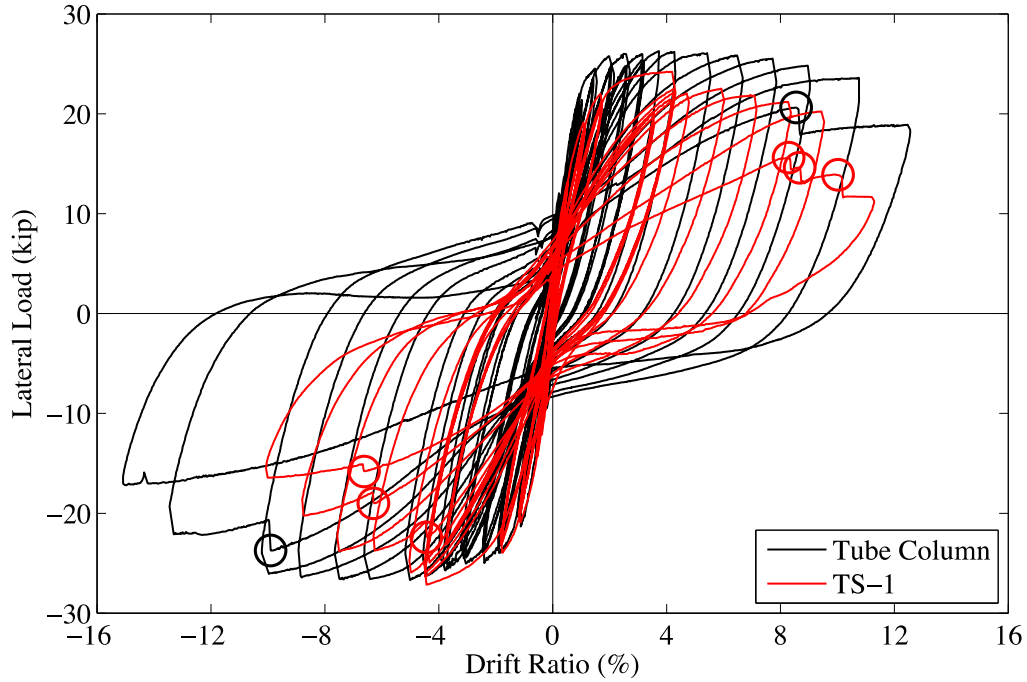


Figure 4.16 Complete lateral load-drift ratio response of tube column and TS-1. Circle markers indicate points of longitudinal rebar fracture.

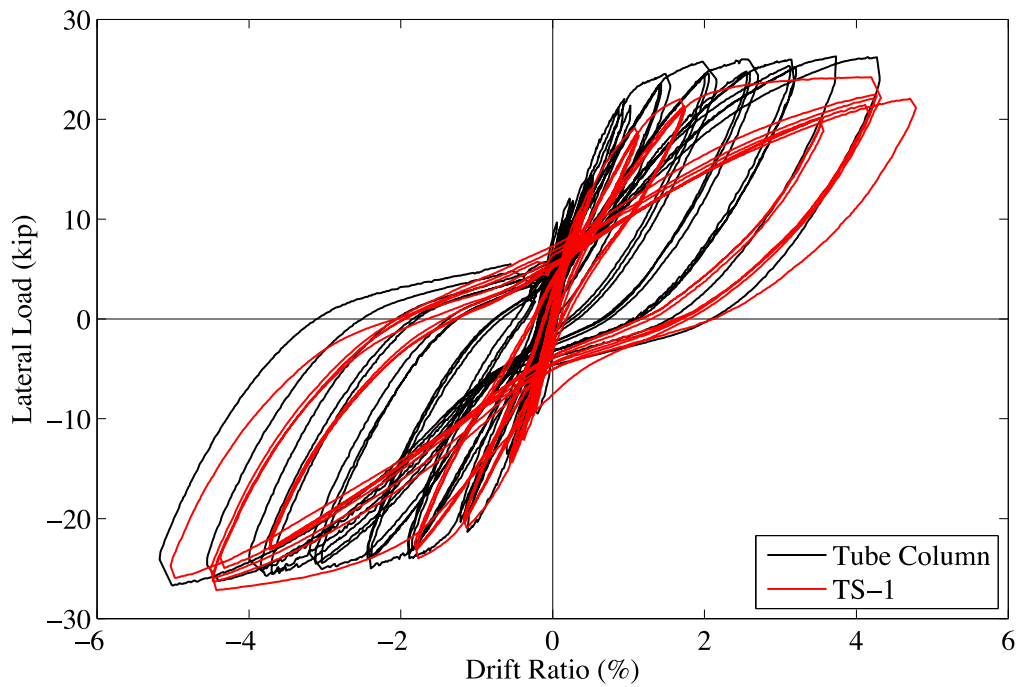


Figure 4.17 Lateral load-drift ratio response of tube column and TS-1, to $\theta_r=4.8\%$.

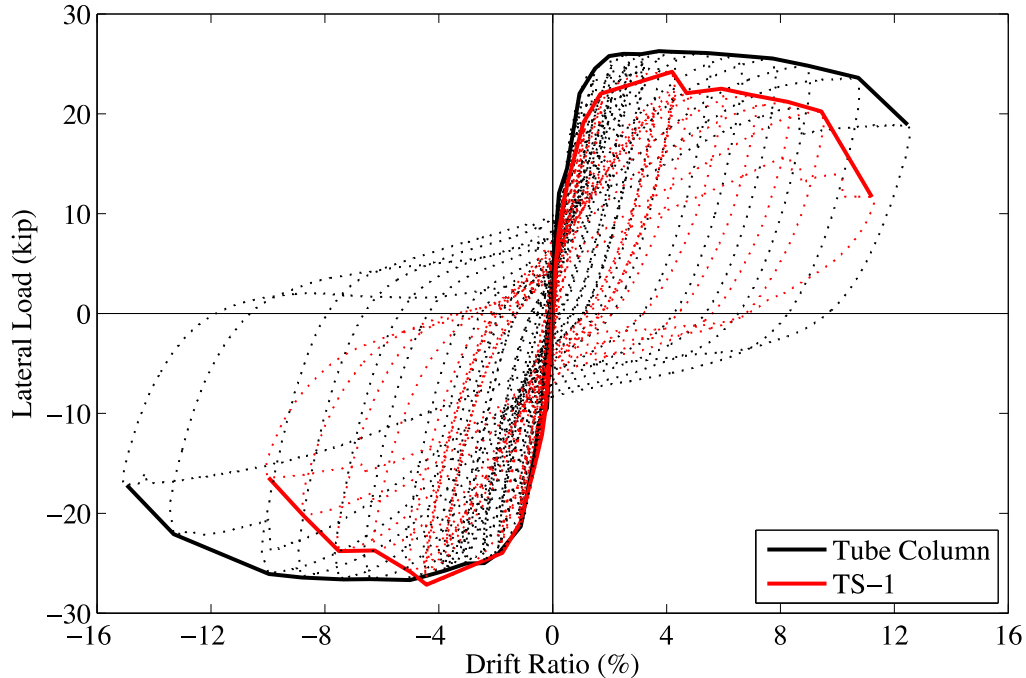


Figure 4.18 Complete lateral load-drift ratio response of tube column and TS-1, with global envelope curve shown for clarity.

By the end of the test, however, the disparity in the load carrying capacity of the columns is evident. TS-1 shows a softening behavior at drift ratios approximately greater than 5%. Though the tube column also shows softening, the reduction in load occurs more gradually over a larger range of drift ratios. At a drift ratio of approximately -10.0%, the tube column maintained a capacity of 26.1 kips, while TS-1 maintained a capacity of 16.4 kips, corresponding to 97.7% and 60.6% of maximum column lateral load capacity, respectively. Once it reached a drift ratio of -15.0%, the tube column was only reduced to 17.2 kips, or 64.4% of its maximum capacity. A similar difference in performance at high drift ratios also occurred for eastward loading. The tube column was able to maintain 89.8% of its lateral capacity at a drift ratio of 10.7%, while TS-1 maintained 83.6% of full capacity.

From the hysteresis loop of TS-1, a total of 6 rebar fractures can be observed by the end of the test. The first, second, and third rebar fractures occurred at target drift ratios of 6.0%, 8.3%, and 9.5%, respectively. The final three fractures occurred in the final loading cycle, with a target drift ratio of 11.1%. The tube column performed significantly better than TS-1 in terms of longitudinal rebar fracture. A total of two rebar fractures were observed in the tube column: the first at a target drift ratio of 11.3%, and the final at the target drift ratio of 13.1%.

Compared to TS-1, the tube column may have exhibited higher lateral load capacities at large drift ratios and reduced longitudinal rebar fractures due to its greater compression damage resistance. As previously mentioned, spalling of concrete did not occur in the tube column, and compression damage was limited to splitting cracks at the base of the column (Figure 4.19a). Column TS-1, however, showed localized spalling starting at a drift ratio of 3.6%, with visible buckling observed at a drift ratio of 4.8% (Figure 4.19b). This localized damage was attributed to a construction flaw that caused the cover thickness of TS-1 to be very thin. Although the tube column had a higher design concrete cover than TS-1 (1 in. compared to 1/2 in.), it may have

been able to delay buckling more effectively in part due to its higher transverse reinforcement over TS-1.

The overall damage resistance of the tube column may be further explained by the presence of fiber-reinforcement. Terzic and Stojadinovic [2010] tested bridge columns made of plain concrete having the same column gross dimensions as the tube column and TS-1, as well as the same longitudinal reinforcing ratio. The transverse reinforcing ratio of Terzic and Stojadinovic's columns were set to 0.75%. The columns also differed in loading protocol, being subjected to lateral loading in two perpendicular axes and did not utilize a rocking mechanism. Figure 4.19c shows significant spalling at the base of Terzic and Stojadinovic's Base45 column after being subjected to 4.0% drift. The specimen was detailed for a displacement ductility of 4.5. The use of HyFRC suggests improved resistance to cover spalling in laterally loaded bridge columns, which may have implications in achieving higher lateral load capacities and lower rehabilitation efforts after seismic events. By using a transverse reinforcing ratio that is typical for plain concrete columns in addition to HyFRC, as is the case for the tube column, significant ductility can be achieved by reducing damage in the column.

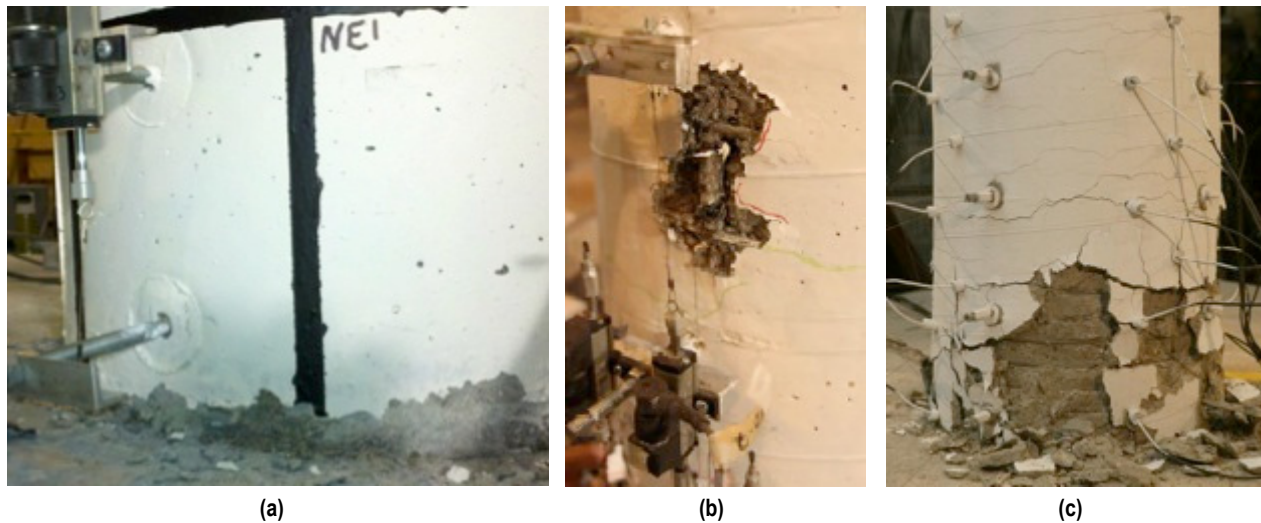


Figure 4.19 Column compression damage: (a) Tube column at 4.8% drift; fine splitting cracks are present on the column surface; (b) TS-1 after 4.8% drift; localized buckling at fabrication flaw is highlighted [Kumar et al. 2011]; and (c) Base45 after 4.0% drift; spalling is extensive at the column base [Terzic and Stojadinovic 2010].

5 Summary and Conclusions

A bridge column design incorporating accelerated bridge construction (ABC) and deterioration reduction through micro- and macrocrack control (DRMC) methodologies was investigated for its constructability and seismic performance. To incorporate both methodologies, a precast hybrid fiber-reinforced concrete (HyFRC) tube containing the column's longitudinal and transverse reinforcement was fabricated to simulate an element built offsite and later brought to a construction site. After being cast in its foundation, the tube was filled with cast-in-place plain concrete. The use of HyFRC was expected to significantly enhance the column's ductility during seismic loading. To accommodate nonlinear deformations, the tube column utilized a base-rocking behavior by unbonding the longitudinal rebar from the concrete near the column base.

The column was subjected to static, uni-directional cyclic lateral loading. Despite limiting the HyFRC to the precast tube, the column generally achieved equivalent or greater lateral load capacity when compared to a fully cast-in-place HyFRC column of similar dimensions and seismic testing protocol. In addition, the tube column showed excellent compression damage resistance as no spalling of concrete was observed, even when the column achieved a drift ratio as high as 13.1%. Fracture of longitudinal rebar also did not occur until reaching a drift of 9.5%.

Use of a precast tube eliminated concerns about the reduced cast-in-place workability of fiber-reinforced concrete in reinforced concrete structural elements. The presented tube column design allows for a practical method of utilizing HyFRC, while obtaining the full crack-resisting benefits of HyFRC.

REFERENCES

- American Society of Civil Engineers (2013). Report Card for America's Infrastructure, from <http://www.infrastructurereportcard.org>.
- ASTM Standard C1609 (2006). Standard test method for flexural performance of fiber-reinforced concrete, West Conshohocken, PA.
- Billington S.L., Yoon J.K. (2004). Cyclic response of unbonded posttensioned precast columns with ductile fiber-reinforced concrete, *J. Bridge Eng.*, 9(4): 353–363.
- Blunt J., Ostertag C.P. (2009a). Deflection hardening and workability of hybrid fiber composites, *ACI Mater. J.*, 106(3): 265–272.
- Blunt J., Ostertag, C.P. (2009b). Performance-based approach for the design of a deflection hardened hybrid fiber-reinforced concrete, *J. Eng. Mech.*, 135(9): 978–986.
- Culmo M. P. (2011). Accelerated Bridge Construction, *Federal Highway Administration*, Springfield, VA.
- Grubb J.A., Blunt J., Ostertag C.P., Devine T.M. (2007). Effect of steel microfibers on corrosion of steel reinforcing bars, *Cement Concrete Res.*, 37(7): 1115–1126.
- Hieber D.G., Wacker, J.M., Eberhard, M.O., Stanton, J.F. (2005). State-of-the-art report on precast concrete systems for rapid construction of bridges.
- Ketchum M., Chang V., Shantz T. (2004). Influence of design ground motion level on highway bridge costs, *Project No. 6D01*, Program of Applied Earthquake Engineering Research on Lifeline Systems, Pacific Earthquake Engineering Research Center, University of California, Berkeley, CA.
- Kwan W.-P., Billington S.L. (2003a). Unbonded posttensioned concrete bridge piers. I: Monotonic and cyclic analyses. *J. Bridge Eng.*, 8(2): 92–101.
- Kwan W.-P., Billington S.L. (2003b). Unbonded posttensioned concrete bridge piers. II: Seismic analyses, *J. Bridge Eng.*, 8(2): 102–111.
- Kumar P., Jen G., Trono W., Panagiotou M., Ostertag, C.P. (2011). Self compacting hybrid fiber reinforced concrete composites for bridge columns, *PEER Report No. 2011/106*, Pacific Earthquake Engineering Research Center, University of California, Berkeley, CA.
- Ostertag C.P., Blunt J. (2010). Effect of crack control in hybrid fiber reinforced concrete composites on corrosion rate of steel reinforcing bars, *Proc. Monogr. Eng. Wate.*, 2: 894–900.
- Panagiotou M., Trono W., Jen G., Kumar P., Ostertag C.P. (2014). Experimental seismic response of hybrid fiber-reinforced concrete bridge columns with novel longitudinal reinforcing detailing, *J. Bridge Eng.*, doi: 10.1061/(ASCE)BE.1943-5592.0000684.
- Terzic V., Stojadinovic B. (2010). Post-earthquake traffic capacity of modern bridges in California, *PEER Report No. 2010/103*, Pacific Earthquake Engineering Research Center, University of California, Berkeley, CA.
- Trono W., Jen G., Panagiotou M., Scheottler M., Ostertag C.P. (2014). Seismic response of a damage-resistant recentering posttensioned-HyFRC bridge column, *J. Bridge Eng.*, doi: 10.1061/(ASCE)BE.1943-5592.0000692.
- Yi C.K., Ostertag, C.P. (2005). Mechanical approach in mitigating alkali-silica reaction. *Cement Concrete Res.*, 35(1): 67–75.

Appendix A Column Mix Designs

Table A.1 Tube HyFRC SSD Mix Proportions (1 yd³).

Material	Weight / Volume
Cement Type I/II (lb)	825
Fly Ash Type F (lb)	275
Sand (lb)	2201
8mm PVA Fiber (lb)	4.4
30mm Steel Fiber (lb)	239
Batched Water (lb)	359
Superplasticizer (lb / L)	12.0 / 5.19
VMA (lb / L)	17.5 / 7.92

Table A.2 Tube HyFRC SSD Mix Proportion Ratios

Material	Ratio
Fly Ash / Cementitious	0.25
Water / Cementitious	0.35
PVA Fiber Volume (%)	0.20
Steel Fiber Volume (%)	1.80
SP Dosage (fl oz / cwt)	16.0
SP Wt-% Binder	1.09
VMA Dosage (fl oz / cwt)	24.4
VMA Wt-% Binder	1.59

Table A.3 Tube HyFRC batched mix proportions (0.33 yd³).

Material	Weight / Volume
Cement Type I/II (lb)	275
Fly Ash Type F (lb)	92
Sand ^a (lb)	775
8mm PVA Fiber (lb)	1.5
30mm Steel Fiber (lb)	80
Batched Water (lb)	99
Superplasticizer (L)	1.73
VMA (L)	2.64

(a) Free moisture: +2.80%

Table A.4 Core concrete SSD mix proportions (1 yd³).

Material	Weight
Cement Type I/II (lb)	802
Sand (lb)	1477
3/8" Pea Gravel (lb)	1168
Batched Water (lb)	385

Table A.5 Core concrete SSD mix proportion ratios.

Material	Ratio
Water / Cementitious	0.48

Table A.6 Core concrete batched mix proportions (0.20 yd³).

Material	Weight
Cement Type I/II (lb)	158
Sand ^a (lb)	301
3/8" Pea Gravel ^b (lb)	229
Batched Water (lb)	68

(a) Free moisture: +3.20%

(b) Free moisture: -0.80%

Appendix B Response History of Vertical Displacement Transducers and Strain Gauges

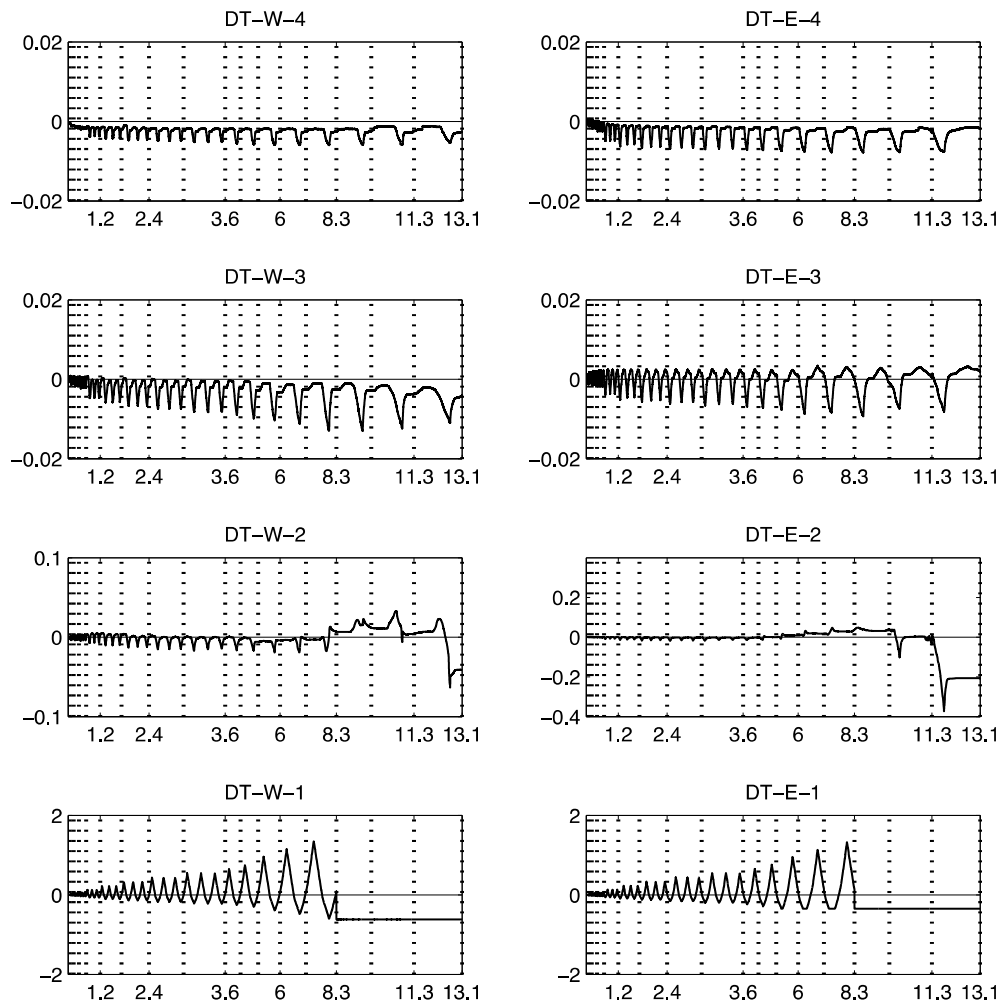


Figure B.1 Displacement transducer measurements on western and eastern column faces. X-axis is in drift ratio (%); Y-axis is in displacement (in.).

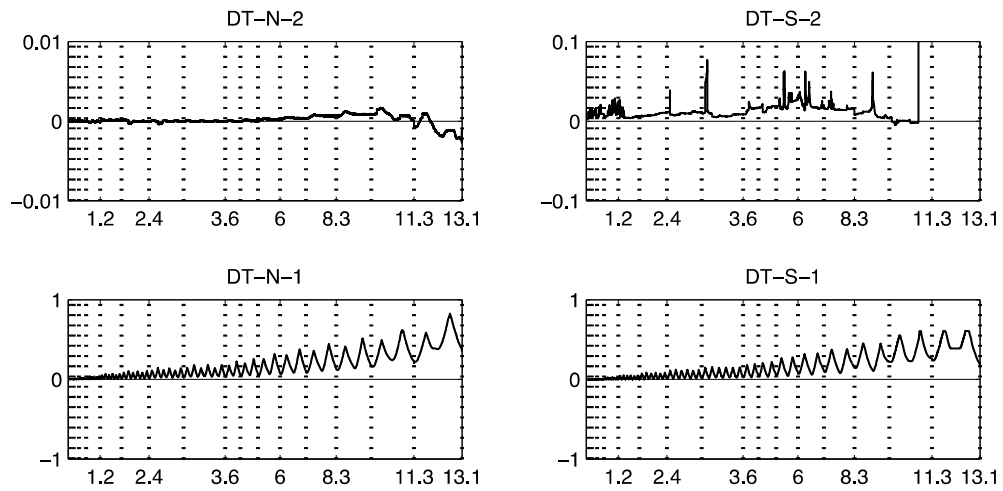


Figure B.2 Displacement transducer measurements on northern and southern column faces. X-axis is in drift ratio (%); Y-axis is in displacement (in.).

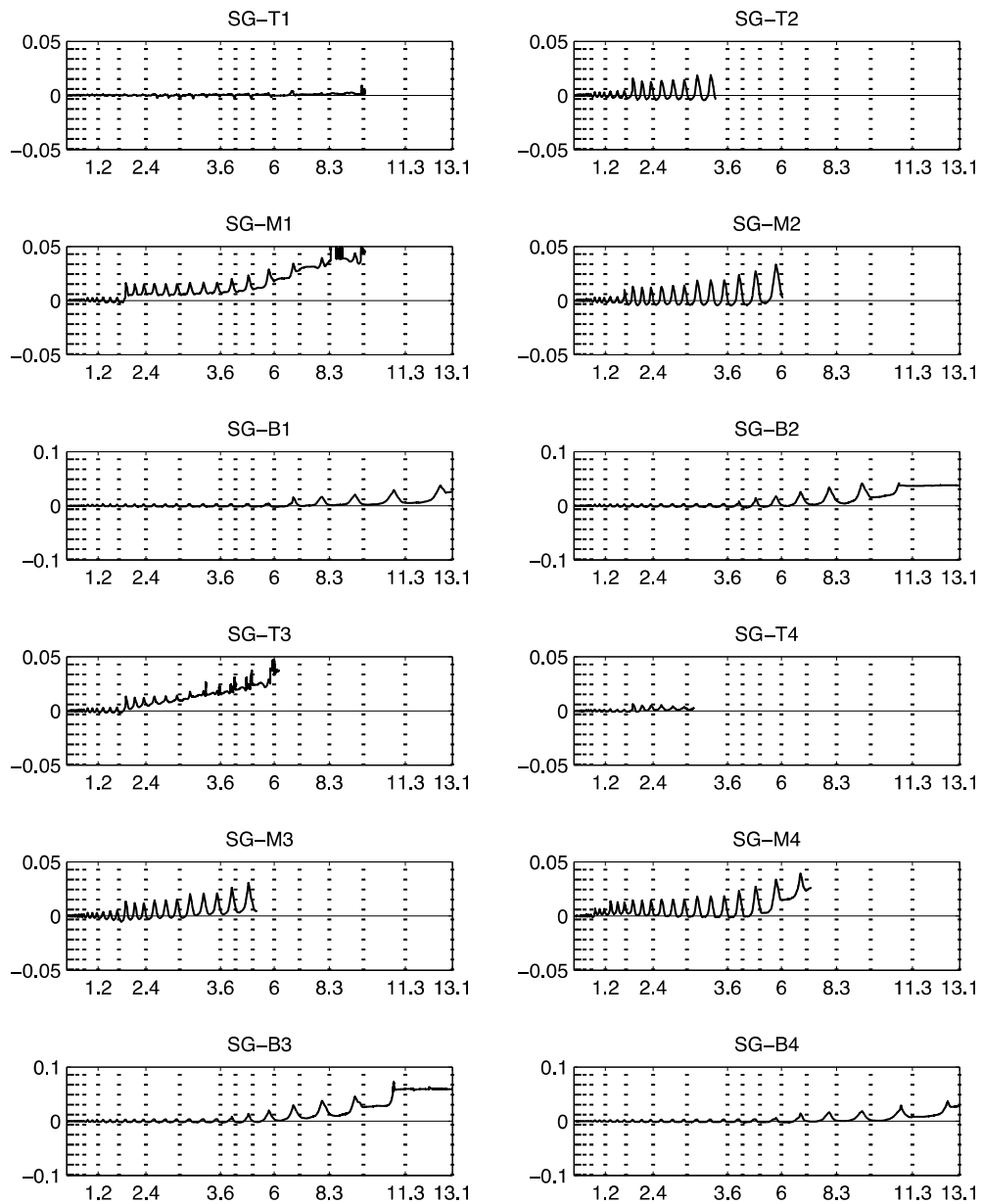


Figure B.3 Strain gauge measurements from column west face rebar. X-axis is in drift ratio (%); Y-axis is in strain (in./in.).

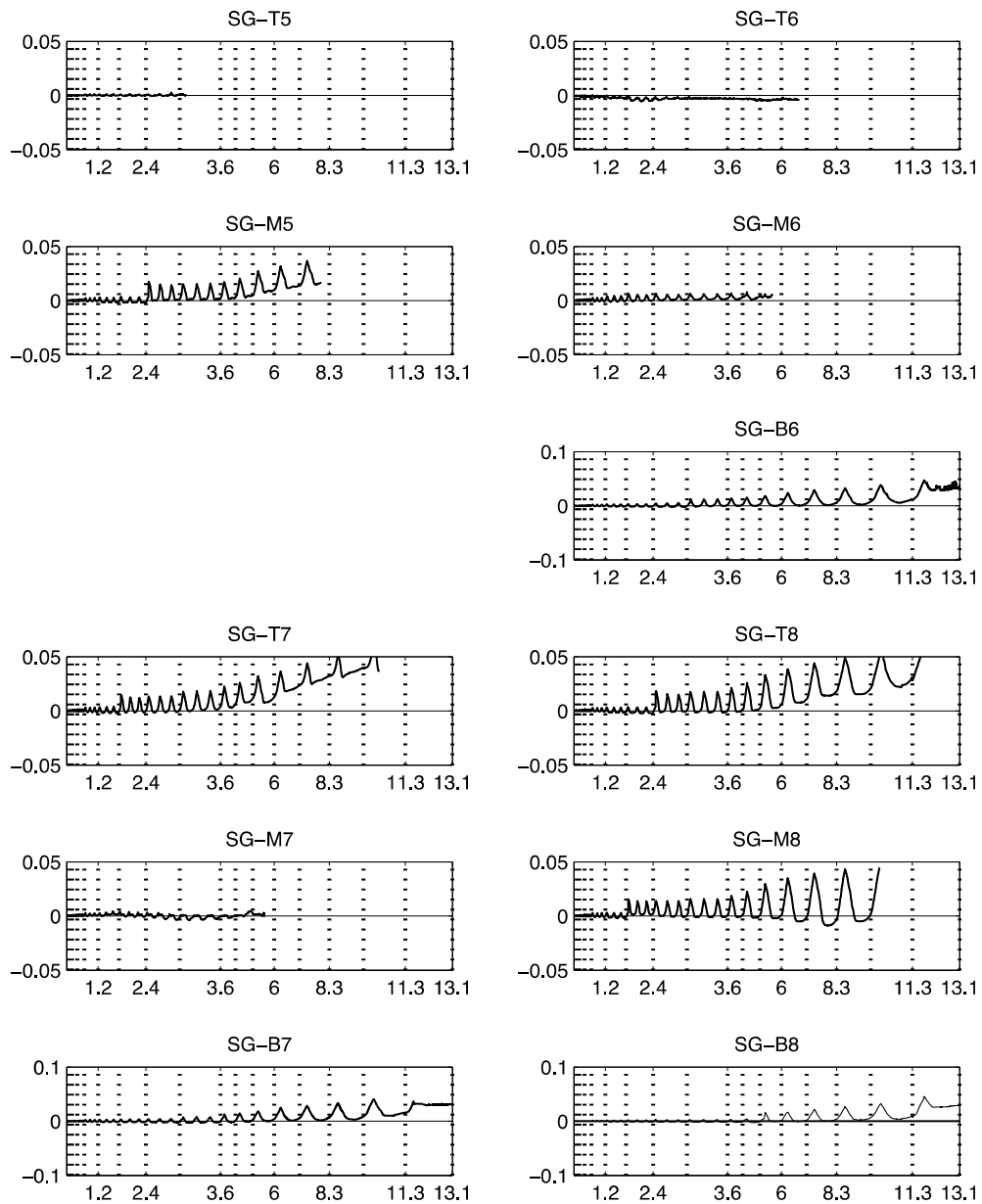


Figure B.4 Strain gauge measurements from column east face rebar. X-axis is in drift ratio (%); Y-axis is in strain (in./in.). Measurements from SG-B5 were not obtained.

PEER REPORTS

PEER reports are available as a free PDF download from http://peer.berkeley.edu/publications/peer_reports_complete.html. Printed hard copies of PEER reports can be ordered directly from our printer by following the instructions at http://peer.berkeley.edu/publications/peer_reports.html. For other related questions about the PEER Report Series, contact the Pacific Earthquake Engineering Research Center, 325 Davis Hall mail code 1792, Berkeley, CA 94720. Tel.: (510) 642-3437; Fax: (510) 665-1655; Email: peer_editor@berkeley.edu

- PEER 2014/19** *Seismic Response of a Hybrid Fiber-Reinforced Concrete Bridge Column Detailed for Accelerated Bridge Construction.* Wilson Nguyen, William Trono, Marios Panagiotou, and Claudia P. Ostertag. December 2014.
- PEER 2014/18** *Three-Dimensional Beam-Truss Model for Reinforced Concrete Walls and Slabs Subjected to Cyclic Static or Dynamic Loading.* Yuan Lu, Marios Panagiotou, and Ioannis Koutromanos. December 2014.
- PEER 2014/17** *PEER NGA-East Database.* Christine A. Goulet, Tadahiro Kishida, Timothy D. Ancheta, Chris H. Cramer, Robert B. Darragh, Walter J. Silva, Youssef M.A. Hashash, Joseph Harmon, Jonathan P. Stewart, Katie E. Wooddell, and Robert R. Youngs. October 2014.
- PEER 2014/16** *Guidelines for Performing Hazard-Consistent One-Dimensional Ground Response Analysis for Ground Motion Prediction.* Jonathan P. Stewart, Kioumars Afshari, and Youssef M.A. Hashash. October 2014.
- PEER 2014/15** *NGA-East Regionalization Report: Comparison of Four Crustal Regions within Central and Eastern North America using Waveform Modeling and 5%-Damped Pseudo-Spectral Acceleration Response.* Jennifer Dreiling, Marius P. Isken, Walter D. Mooney, Martin C. Chapman, and Richard W. Godbee. October 2014.
- PEER 2014/14** *Scaling Relations between Seismic Moment and Rupture Area of Earthquakes in Stable Continental Regions.* Paul Somerville. August 2014.
- PEER 2014/13** *PEER Preliminary Notes and Observations on the August 24, 2014, South Napa Earthquake.* Grace S. Kang (Editor), Stephen A. Mahin (Editors). September 2014.
- PEER 2014/12** *Reference-Rock Site Conditions for Central and Eastern North America: Part II – Attenuation (Kappa) Definition.* Kenneth W. Campbell, Youssef M.A. Hashash, Byungmin Kim, Albert R. Kottke, Ellen M. Rathje, Walter J. Silva, and Jonathan P. Stewart. August 2014.
- PEER 2014/11** *Reference-Rock Site Conditions for Central and Eastern North America: Part I - Velocity Definition.* Youssef M.A. Hashash, Albert R. Kottke, Jonathan P. Stewart, Kenneth W. Campbell, Byungmin Kim, Ellen M. Rathje, Walter J. Silva, Sissy Nikolaou, and Cheryl Moss. August 2014.
- PEER 2014/10** *Evaluation of Collapse and Non-Collapse of Parallel Bridges Affected by Liquefaction and Lateral Spreading.* Benjamin Turner, Scott J. Brandenberg, and Jonathan P. Stewart. August 2014.
- PEER 2014/09** *PEER Arizona Strong-Motion Database and GMPEs Evaluation.* Tadahiro Kishida, Robert E. Kayen, Olga-Joan Ktenidou, Walter J. Silva, Robert B. Darragh, and Jennie Watson-Lamprey. June 2014.
- PEER 2014/08** *Unbonded Pretensioned Bridge Columns with Rocking Detail.* Jeffrey A. Schaefer, Bryan Kennedy, Marc O. Eberhard, John F. Stanton. June 2014.
- PEER 2014/07** *Northridge 20 Symposium Summary Report: Impacts, Outcomes, and Next Steps.* May 2014.
- PEER 2014/06** *Report of the Tenth Planning Meeting of NEES/E-Defense Collaborative Research on Earthquake Engineering.* December 2013.
- PEER 2014/05** *Seismic Velocity Site Characterization of Thirty-One Chilean Seismometer Stations by Spectral Analysis of Surface Wave Dispersion.* Robert Kayen, Brad D. Carkin, Skye Corbet, Camilo Pinilla, Allan Ng, Edward Gorbis, and Christine Truong. April 2014.
- PEER 2014/04** *Effect of Vertical Acceleration on Shear Strength of Reinforced Concrete Columns.* Hyerin Lee and Khalid M. Mosalam. April 2014.
- PEER 2014/03** *Retest of Thirty-Year-Old Neoprene Isolation Bearings.* James M. Kelly and Niel C. Van Engelen. March 2014.
- PEER 2014/02** *Theoretical Development of Hybrid Simulation Applied to Plate Structures.* Ahmed A. Bakhaty, Khalid M. Mosalam, and Sanjay Govindjee. January 2014.
- PEER 2014/01** *Performance-Based Seismic Assessment of Skewed Bridges.* Peyman Kaviani, Farzin Zareian, and Ertugrul Taciroglu. January 2014.
- PEER 2013/26** *Urban Earthquake Engineering. Proceedings of the U.S.-Iran Seismic Workshop.* December 2013.

- PEER 2013/25** *Earthquake Engineering for Resilient Communities: 2013 PEER Internship Program Research Report Collection.* Heidi Tremayne (Editor), Stephen A. Mahin (Editor), Jorge Archbold Monterossa, Matt Brosman, Shelly Dean, Katherine deLaveaga, Curtis Fong, Donovan Holder, Rakeeb Khan, Elizabeth Jachens, David Lam, Daniela Martinez Lopez, Mara Minner, Geffen Oren, Julia Pavicic, Melissa Quinonez, Lorena Rodriguez, Sean Salazar, Kelli Slaven, Vivian Steyert, Jenny Taing, and Salvador Tena. December 2013.
- PEER 2013/24** *NGA-West2 Ground Motion Prediction Equations for Vertical Ground Motions.* September 2013.
- PEER 2013/23** *Coordinated Planning and Preparedness for Fire Following Major Earthquakes.* Charles Scawthorn. November 2013.
- PEER 2013/22** *GEM-PEER Task 3 Project: Selection of a Global Set of Ground Motion Prediction Equations.* Jonathan P. Stewart, John Douglas, Mohammad B. Javanbarg, Carola Di Alessandro, Yousef Bozorgnia, Norman A. Abrahamson, David M. Boore, Kenneth W. Campbell, Elise Delavaud, Mustafa Erdik and Peter J. Stafford. December 2013.
- PEER 2013/21** *Seismic Design and Performance of Bridges with Columns on Rocking Foundations.* Grigorios Antonellis and Marios Panagiotou. September 2013.
- PEER 2013/20** *Experimental and Analytical Studies on the Seismic Behavior of Conventional and Hybrid Braced Frames.* Jiun-Wei Lai and Stephen A. Mahin. September 2013.
- PEER 2013/19** *Toward Resilient Communities: A Performance-Based Engineering Framework for Design and Evaluation of the Built Environment.* Michael William Mieler, Bozidar Stojadinovic, Robert J. Budnitz, Stephen A. Mahin and Mary C. Comerio. September 2013.
- PEER 2013/18** *Identification of Site Parameters that Improve Predictions of Site Amplification.* Ellen M. Rathje and Sara Navidi. July 2013.
- PEER 2013/17** *Response Spectrum Analysis of Concrete Gravity Dams Including Dam-Water-Foundation Interaction.* Arnkjell Løkke and Anil K. Chopra. July 2013.
- PEER 2013/16** *Effect of hoop reinforcement spacing on the cyclic response of large reinforced concrete special moment frame beams.* Marios Panagiotou, Tea Visnjic, Grigorios Antonellis, Panagiotis Galanis, and Jack P. Moehle. June 2013.
- PEER 2013/15** *A Probabilistic Framework to Include the Effects of Near-Fault Directivity in Seismic Hazard Assessment.* Shrey Kumar Shahi, Jack W. Baker. October 2013.
- PEER 2013/14** *Hanging-Wall Scaling using Finite-Fault Simulations.* Jennifer L. Donahue and Norman A. Abrahamson. September 2013.
- PEER 2013/13** *Semi-Empirical Nonlinear Site Amplification and its Application in NEHRP Site Factors.* Jonathan P. Stewart and Emel Seyhan. November 2013.
- PEER 2013/12** *Nonlinear Horizontal Site Response for the NGA-West2 Project.* Ronnie Kamai, Norman A. Abramson, Walter J. Silva. May 2013.
- PEER 2013/11** *Epistemic Uncertainty for NGA-West2 Models.* Linda Al Atik and Robert R. Youngs. May 2013.
- PEER 2013/10** *NGA-West 2 Models for Ground-Motion Directionality.* Shrey K. Shahi and Jack W. Baker. May 2013.
- PEER 2013/09** *Final Report of the NGA-West2 Directivity Working Group.* Paul Spudich, Jeffrey R. Bayless, Jack W. Baker, Brian S.J. Chiou, Badie Rowshandel, Shrey Shahi, and Paul Somerville. May 2013.
- PEER 2013/08** *NGA-West2 Model for Estimating Average Horizontal Values of Pseudo-Absolute Spectral Accelerations Generated by Crustal Earthquakes.* I. M. Idriss. May 2013.
- PEER 2013/07** *Update of the Chiou and Youngs NGA Ground Motion Model for Average Horizontal Component of Peak Ground Motion and Response Spectra.* Brian Chiou and Robert Youngs. May 2013.
- PEER 2013/06** *NGA-West2 Campbell-Bozorgnia Ground Motion Model for the Horizontal Components of PGA, PGV, and 5%-Damped Elastic Pseudo-Acceleration Response Spectra for Periods Ranging from 0.01 to 10 sec.* Kenneth W. Campbell and Yousef Bozorgnia. May 2013.
- PEER 2013/05** *NGA-West 2 Equations for Predicting Response Spectral Accelerations for Shallow Crustal Earthquakes.* David M. Boore, Jonathan P. Stewart, Emel Seyhan, Gail M. Atkinson. May 2013.
- PEER 2013/04** *Update of the AS08 Ground-Motion Prediction Equations Based on the NGA-West2 Data Set.* Norman Abrahamson, Walter Silva, and Ronnie Kamai. May 2013.
- PEER 2013/03** *PEER NGA-West2 Database.* Timothy D. Ancheta, Robert B. Darragh, Jonathan P. Stewart, Emel Seyhan, Walter J. Silva, Brian S.J. Chiou, Katie E. Wooddell, Robert W. Graves, Albert R. Kottke, David M. Boore, Tadahiro Kishida, and Jennifer L. Donahue. May 2013.

- PEER 2013/02** *Hybrid Simulation of the Seismic Response of Squat Reinforced Concrete Shear Walls.* Catherine A. Whyte and Božidar Stojadinovic. May 2013.
- PEER 2013/01** *Housing Recovery in Chile: A Qualitative Mid-program Review.* Mary C. Comerio. February 2013.
- PEER 2012/08** *Guidelines for Estimation of Shear Wave Velocity.* Bernard R. Wair, Jason T. DeJong, and Thomas Shantz. December 2012.
- PEER 2012/07** *Earthquake Engineering for Resilient Communities: 2012 PEER Internship Program Research Report Collection.* Heidi Tremayne (Editor), Stephen A. Mahin (Editor), Collin Anderson, Dustin Cook, Michael Erceg, Carlos Esparza, Jose Jimenez, Dorian Krausz, Andrew Lo, Stephanie Lopez, Nicole McCurdy, Paul Shipman, Alexander Strum, Eduardo Vega. December 2012.
- PEER 2012/06** *Fragilities for Precarious Rocks at Yucca Mountain.* Matthew D. Purvance, Rasool Anooshehpour, and James N. Brune. December 2012.
- PEER 2012/05** *Development of Simplified Analysis Procedure for Piles in Laterally Spreading Layered Soils.* Christopher R. McGann, Pedro Arduino, and Peter Mackenzie-Helnwein. December 2012.
- PEER 2012/04** *Unbonded Pre-Tensioned Columns for Bridges in Seismic Regions.* Phillip M. Davis, Todd M. Janes, Marc O. Eberhard, and John F. Stanton. December 2012.
- PEER 2012/03** *Experimental and Analytical Studies on Reinforced Concrete Buildings with Seismically Vulnerable Beam-Column Joints.* Sangjoon Park and Khalid M. Mosalam. October 2012.
- PEER 2012/02** *Seismic Performance of Reinforced Concrete Bridges Allowed to Uplift during Multi-Directional Excitation.* Andres Oscar Espinoza and Stephen A. Mahin. July 2012.
- PEER 2012/01** *Spectral Damping Scaling Factors for Shallow Crustal Earthquakes in Active Tectonic Regions.* Sanaz Rezaeian, Yousef Bozorgnia, I. M. Idriss, Kenneth Campbell, Norman Abrahamson, and Walter Silva. July 2012.
- PEER 2011/10** *Earthquake Engineering for Resilient Communities: 2011 PEER Internship Program Research Report Collection.* Eds. Heidi Faison and Stephen A. Mahin. December 2011.
- PEER 2011/09** *Calibration of Semi-Stochastic Procedure for Simulating High-Frequency Ground Motions.* Jonathan P. Stewart, Emel Seyhan, and Robert W. Graves. December 2011.
- PEER 2011/08** *Water Supply in regard to Fire Following Earthquake.* Charles Scawthorn. November 2011.
- PEER 2011/07** *Seismic Risk Management in Urban Areas. Proceedings of a U.S.-Iran-Turkey Seismic Workshop.* September 2011.
- PEER 2011/06** *The Use of Base Isolation Systems to Achieve Complex Seismic Performance Objectives.* Troy A. Morgan and Stephen A. Mahin. July 2011.
- PEER 2011/05** *Case Studies of the Seismic Performance of Tall Buildings Designed by Alternative Means.* Task 12 Report for the Tall Buildings Initiative. Jack Moehle, Yousef Bozorgnia, Nirmal Jayaram, Pierson Jones, Mohsen Rahnama, Nilesh Shome, Zeynep Tuna, John Wallace, Tony Yang, and Farzin Zareian. July 2011.
- PEER 2011/04** *Recommended Design Practice for Pile Foundations in Laterally Spreading Ground.* Scott A. Ashford, Ross W. Boulanger, and Scott J. Brandenberg. June 2011.
- PEER 2011/03** *New Ground Motion Selection Procedures and Selected Motions for the PEER Transportation Research Program.* Jack W. Baker, Ting Lin, Shrey K. Shahi, and Nirmal Jayaram. March 2011.
- PEER 2011/02** *A Bayesian Network Methodology for Infrastructure Seismic Risk Assessment and Decision Support.* Michelle T. Bensi, Armen Der Kiureghian, and Daniel Straub. March 2011.
- PEER 2011/01** *Demand Fragility Surfaces for Bridges in Liquefied and Laterally Spreading Ground.* Scott J. Brandenberg, Jian Zhang, Pirooz Kashighandi, Yili Huo, and Minxing Zhao. March 2011.
- PEER 2010/05** *Guidelines for Performance-Based Seismic Design of Tall Buildings.* Developed by the Tall Buildings Initiative. November 2010.
- PEER 2010/04** *Application Guide for the Design of Flexible and Rigid Bus Connections between Substation Equipment Subjected to Earthquakes.* Jean-Bernard Dastous and Armen Der Kiureghian. September 2010.
- PEER 2010/03** *Shear Wave Velocity as a Statistical Function of Standard Penetration Test Resistance and Vertical Effective Stress at Caltrans Bridge Sites.* Scott J. Brandenberg, Naresh Bellana, and Thomas Shantz. June 2010.
- PEER 2010/02** *Stochastic Modeling and Simulation of Ground Motions for Performance-Based Earthquake Engineering.* Sanaz Rezaeian and Armen Der Kiureghian. June 2010.
- PEER 2010/01** *Structural Response and Cost Characterization of Bridge Construction Using Seismic Performance Enhancement Strategies.* Ady Aviram, Božidar Stojadinović, Gustavo J. Parra-Montesinos, and Kevin R. Mackie. March 2010.

- PEER 2009/03** *The Integration of Experimental and Simulation Data in the Study of Reinforced Concrete Bridge Systems Including Soil-Foundation-Structure Interaction.* Matthew Dryden and Gregory L. Fenves. November 2009.
- PEER 2009/02** *Improving Earthquake Mitigation through Innovations and Applications in Seismic Science, Engineering, Communication, and Response. Proceedings of a U.S.-Iran Seismic Workshop.* October 2009.
- PEER 2009/01** *Evaluation of Ground Motion Selection and Modification Methods: Predicting Median Interstory Drift Response of Buildings.* Curt B. Haselton, Ed. June 2009.
- PEER 2008/10** *Technical Manual for Strata.* Albert R. Kottke and Ellen M. Rathje. February 2009.
- PEER 2008/09** *NGA Model for Average Horizontal Component of Peak Ground Motion and Response Spectra.* Brian S.-J. Chiou and Robert R. Youngs. November 2008.
- PEER 2008/08** *Toward Earthquake-Resistant Design of Concentrically Braced Steel Structures.* Patxi Uriz and Stephen A. Mahin. November 2008.
- PEER 2008/07** *Using OpenSees for Performance-Based Evaluation of Bridges on Liquefiable Soils.* Stephen L. Kramer, Pedro Arduino, and HyungSuk Shin. November 2008.
- PEER 2008/06** *Shaking Table Tests and Numerical Investigation of Self-Centering Reinforced Concrete Bridge Columns.* Hyung IL Jeong, Junichi Sakai, and Stephen A. Mahin. September 2008.
- PEER 2008/05** *Performance-Based Earthquake Engineering Design Evaluation Procedure for Bridge Foundations Undergoing Liquefaction-Induced Lateral Ground Displacement.* Christian A. Ledezma and Jonathan D. Bray. August 2008.
- PEER 2008/04** *Benchmarking of Nonlinear Geotechnical Ground Response Analysis Procedures.* Jonathan P. Stewart, Annie On-Lei Kwok, Youssef M. A. Hashash, Neven Matasovic, Robert Pyke, Zhiliang Wang, and Zhaohui Yang. August 2008.
- PEER 2008/03** *Guidelines for Nonlinear Analysis of Bridge Structures in California.* Ady Aviram, Kevin R. Mackie, and Božidar Stojadinović. August 2008.
- PEER 2008/02** *Treatment of Uncertainties in Seismic-Risk Analysis of Transportation Systems.* Evangelos Stergiou and Anne S. Kiremidjian. July 2008.
- PEER 2008/01** *Seismic Performance Objectives for Tall Buildings.* William T. Holmes, Charles Kircher, William Petak, and Nabih Youssef. August 2008.
- PEER 2007/12** *An Assessment to Benchmark the Seismic Performance of a Code-Conforming Reinforced Concrete Moment-Frame Building.* Curt Haselton, Christine A. Goulet, Judith Mitrani-Reiser, James L. Beck, Gregory G. Deierlein, Keith A. Porter, Jonathan P. Stewart, and Ertugrul Taciroglu. August 2008.
- PEER 2007/11** *Bar Buckling in Reinforced Concrete Bridge Columns.* Wayne A. Brown, Dawn E. Lehman, and John F. Stanton. February 2008.
- PEER 2007/10** *Computational Modeling of Progressive Collapse in Reinforced Concrete Frame Structures.* Mohamed M. Talaat and Khalid M. Mosalam. May 2008.
- PEER 2007/09** *Integrated Probabilistic Performance-Based Evaluation of Benchmark Reinforced Concrete Bridges.* Kevin R. Mackie, John-Michael Wong, and Božidar Stojadinović. January 2008.
- PEER 2007/08** *Assessing Seismic Collapse Safety of Modern Reinforced Concrete Moment-Frame Buildings.* Curt B. Haselton and Gregory G. Deierlein. February 2008.
- PEER 2007/07** *Performance Modeling Strategies for Modern Reinforced Concrete Bridge Columns.* Michael P. Berry and Marc O. Eberhard. April 2008.
- PEER 2007/06** *Development of Improved Procedures for Seismic Design of Buried and Partially Buried Structures.* Linda Al Atik and Nicholas Sitar. June 2007.
- PEER 2007/05** *Uncertainty and Correlation in Seismic Risk Assessment of Transportation Systems.* Renee G. Lee and Anne S. Kiremidjian. July 2007.
- PEER 2007/04** *Numerical Models for Analysis and Performance-Based Design of Shallow Foundations Subjected to Seismic Loading.* Sivapalan Gajan, Tara C. Hutchinson, Bruce L. Kutter, Prishati Raychowdhury, José A. Ugalde, and Jonathan P. Stewart. May 2008.
- PEER 2007/03** *Beam-Column Element Model Calibrated for Predicting Flexural Response Leading to Global Collapse of RC Frame Buildings.* Curt B. Haselton, Abbie B. Liel, Sarah Taylor Lange, and Gregory G. Deierlein. May 2008.
- PEER 2007/02** *Campbell-Bozorgnia NGA Ground Motion Relations for the Geometric Mean Horizontal Component of Peak and Spectral Ground Motion Parameters.* Kenneth W. Campbell and Yousef Bozorgnia. May 2007.
- PEER 2007/01** *Boore-Atkinson NGA Ground Motion Relations for the Geometric Mean Horizontal Component of Peak and Spectral Ground Motion Parameters.* David M. Boore and Gail M. Atkinson. May 2007.

- PEER 2006/12** *Societal Implications of Performance-Based Earthquake Engineering.* Peter J. May. May 2007.
- PEER 2006/11** *Probabilistic Seismic Demand Analysis Using Advanced Ground Motion Intensity Measures, Attenuation Relationships, and Near-Fault Effects.* Polsak Tothong and C. Allin Cornell. March 2007.
- PEER 2006/10** *Application of the PEER PBEE Methodology to the I-880 Viaduct.* Sashi Kunnath. February 2007.
- PEER 2006/09** *Quantifying Economic Losses from Travel Forgone Following a Large Metropolitan Earthquake.* James Moore, Sungbin Cho, Yue Yue Fan, and Stuart Werner. November 2006.
- PEER 2006/08** *Vector-Valued Ground Motion Intensity Measures for Probabilistic Seismic Demand Analysis.* Jack W. Baker and C. Allin Cornell. October 2006.
- PEER 2006/07** *Analytical Modeling of Reinforced Concrete Walls for Predicting Flexural and Coupled-Shear-Flexural Responses.* Kutay Orakcal, Leonardo M. Massone, and John W. Wallace. October 2006.
- PEER 2006/06** *Nonlinear Analysis of a Soil-Drilled Pier System under Static and Dynamic Axial Loading.* Gang Wang and Nicholas Sitar. November 2006.
- PEER 2006/05** *Advanced Seismic Assessment Guidelines.* Paolo Bazzurro, C. Allin Cornell, Charles Menun, Maziar Motahari, and Nicolas Luco. September 2006.
- PEER 2006/04** *Probabilistic Seismic Evaluation of Reinforced Concrete Structural Components and Systems.* Tae Hyung Lee and Khalid M. Mosalam. August 2006.
- PEER 2006/03** *Performance of Lifelines Subjected to Lateral Spreading.* Scott A. Ashford and Teerawut Juirnarongrit. July 2006.
- PEER 2006/02** *Pacific Earthquake Engineering Research Center Highway Demonstration Project.* Anne Kiremidjian, James Moore, Yue Yue Fan, Nesrin Basoz, Ozgur Yazali, and Meredith Williams. April 2006.
- PEER 2006/01** *Bracing Berkeley. A Guide to Seismic Safety on the UC Berkeley Campus.* Mary C. Comerio, Stephen Tobriner, and Ariane Fehrenkamp. January 2006.
- PEER 2005/16** *Seismic Response and Reliability of Electrical Substation Equipment and Systems.* Junho Song, Armen Der Kiureghian, and Jerome L. Sackman. April 2006.
- PEER 2005/15** *CPT-Based Probabilistic Assessment of Seismic Soil Liquefaction Initiation.* R. E. S. Moss, R. B. Seed, R. E. Kayen, J. P. Stewart, and A. Der Kiureghian. April 2006.
- PEER 2005/14** *Workshop on Modeling of Nonlinear Cyclic Load-Deformation Behavior of Shallow Foundations.* Bruce L. Kutter, Geoffrey Martin, Tara Hutchinson, Chad Harden, Sivapalan Gajan, and Justin Phalen. March 2006.
- PEER 2005/13** *Stochastic Characterization and Decision Bases under Time-Dependent Aftershock Risk in Performance-Based Earthquake Engineering.* Gee Liek Yeo and C. Allin Cornell. July 2005.
- PEER 2005/12** *PEER Testbed Study on a Laboratory Building: Exercising Seismic Performance Assessment.* Mary C. Comerio, editor. November 2005.
- PEER 2005/11** *Van Nuys Hotel Building Testbed Report: Exercising Seismic Performance Assessment.* Helmut Krawinkler, editor. October 2005.
- PEER 2005/10** *First NEES/E-Defense Workshop on Collapse Simulation of Reinforced Concrete Building Structures.* September 2005.
- PEER 2005/09** *Test Applications of Advanced Seismic Assessment Guidelines.* Joe Maffei, Karl Telleen, Danya Mohr, William Holmes, and Yuki Nakayama. August 2006.
- PEER 2005/08** *Damage Accumulation in Lightly Confined Reinforced Concrete Bridge Columns.* R. Tyler Ranf, Jared M. Nelson, Zach Price, Marc O. Eberhard, and John F. Stanton. April 2006.
- PEER 2005/07** *Experimental and Analytical Studies on the Seismic Response of Freestanding and Anchored Laboratory Equipment.* Dimitrios Konstantinidis and Nicos Makris. January 2005.
- PEER 2005/06** *Global Collapse of Frame Structures under Seismic Excitations.* Luis F. Ibarra and Helmut Krawinkler. September 2005.
- PEER 2005/05** *Performance Characterization of Bench- and Shelf-Mounted Equipment.* Samit Ray Chaudhuri and Tara C. Hutchinson. May 2006.
- PEER 2005/04** *Numerical Modeling of the Nonlinear Cyclic Response of Shallow Foundations.* Chad Harden, Tara Hutchinson, Geoffrey R. Martin, and Bruce L. Kutter. August 2005.
- PEER 2005/03** *A Taxonomy of Building Components for Performance-Based Earthquake Engineering.* Keith A. Porter. September 2005.

- PEER 2005/02** *Fragility Basis for California Highway Overpass Bridge Seismic Decision Making.* Kevin R. Mackie and Božidar Stojadinović. June 2005.
- PEER 2005/01** *Empirical Characterization of Site Conditions on Strong Ground Motion.* Jonathan P. Stewart, Yoojoong Choi, and Robert W. Graves. June 2005.
- PEER 2004/09** *Electrical Substation Equipment Interaction: Experimental Rigid Conductor Studies.* Christopher Stearns and André Filiatrault. February 2005.
- PEER 2004/08** *Seismic Qualification and Fragility Testing of Line Break 550-kV Disconnect Switches.* Shakhzod M. Takhirov, Gregory L. Fenves, and Eric Fujisaki. January 2005.
- PEER 2004/07** *Ground Motions for Earthquake Simulator Qualification of Electrical Substation Equipment.* Shakhzod M. Takhirov, Gregory L. Fenves, Eric Fujisaki, and Don Clyde. January 2005.
- PEER 2004/06** *Performance-Based Regulation and Regulatory Regimes.* Peter J. May and Chris Koski. September 2004.
- PEER 2004/05** *Performance-Based Seismic Design Concepts and Implementation: Proceedings of an International Workshop.* Peter Fajfar and Helmut Krawinkler, editors. September 2004.
- PEER 2004/04** *Seismic Performance of an Instrumented Tilt-up Wall Building.* James C. Anderson and Vitelmo V. Bertero. July 2004.
- PEER 2004/03** *Evaluation and Application of Concrete Tilt-up Assessment Methodologies.* Timothy Graf and James O. Malley. October 2004.
- PEER 2004/02** *Analytical Investigations of New Methods for Reducing Residual Displacements of Reinforced Concrete Bridge Columns.* Junichi Sakai and Stephen A. Mahin. August 2004.
- PEER 2004/01** *Seismic Performance of Masonry Buildings and Design Implications.* Kerri Anne Taeko Tokoro, James C. Anderson, and Vitelmo V. Bertero. February 2004.
- PEER 2003/18** *Performance Models for Flexural Damage in Reinforced Concrete Columns.* Michael Berry and Marc Eberhard. August 2003.
- PEER 2003/17** *Predicting Earthquake Damage in Older Reinforced Concrete Beam-Column Joints.* Catherine Pagni and Laura Lowes. October 2004.
- PEER 2003/16** *Seismic Demands for Performance-Based Design of Bridges.* Kevin Mackie and Božidar Stojadinović. August 2003.
- PEER 2003/15** *Seismic Demands for Nondeteriorating Frame Structures and Their Dependence on Ground Motions.* Ricardo Antonio Medina and Helmut Krawinkler. May 2004.
- PEER 2003/14** *Finite Element Reliability and Sensitivity Methods for Performance-Based Earthquake Engineering.* Terje Haukaas and Armen Der Kiureghian. April 2004.
- PEER 2003/13** *Effects of Connection Hysteretic Degradation on the Seismic Behavior of Steel Moment-Resisting Frames.* Janise E. Rodgers and Stephen A. Mahin. March 2004.
- PEER 2003/12** *Implementation Manual for the Seismic Protection of Laboratory Contents: Format and Case Studies.* William T. Holmes and Mary C. Comerio. October 2003.
- PEER 2003/11** *Fifth U.S.-Japan Workshop on Performance-Based Earthquake Engineering Methodology for Reinforced Concrete Building Structures.* February 2004.
- PEER 2003/10** *A Beam-Column Joint Model for Simulating the Earthquake Response of Reinforced Concrete Frames.* Laura N. Lowes, Nilanjan Mitra, and Arash Altoontash. February 2004.
- PEER 2003/09** *Sequencing Repairs after an Earthquake: An Economic Approach.* Marco Casari and Simon J. Wilkie. April 2004.
- PEER 2003/08** *A Technical Framework for Probability-Based Demand and Capacity Factor Design (DCFD) Seismic Formats.* Fatemeh Jalayer and C. Allin Cornell. November 2003.
- PEER 2003/07** *Uncertainty Specification and Propagation for Loss Estimation Using FOSM Methods.* Jack W. Baker and C. Allin Cornell. September 2003.
- PEER 2003/06** *Performance of Circular Reinforced Concrete Bridge Columns under Bidirectional Earthquake Loading.* Mahmoud M. Hachem, Stephen A. Mahin, and Jack P. Moehle. February 2003.
- PEER 2003/05** *Response Assessment for Building-Specific Loss Estimation.* Eduardo Miranda and Shahram Taghavi. September 2003.
- PEER 2003/04** *Experimental Assessment of Columns with Short Lap Splices Subjected to Cyclic Loads.* Murat Melek, John W. Wallace, and Joel Conte. April 2003.

- PEER 2003/03** *Probabilistic Response Assessment for Building-Specific Loss Estimation.* Eduardo Miranda and Hesameddin Aslani. September 2003.
- PEER 2003/02** *Software Framework for Collaborative Development of Nonlinear Dynamic Analysis Program.* Jun Peng and Kincho H. Law. September 2003.
- PEER 2003/01** *Shake Table Tests and Analytical Studies on the Gravity Load Collapse of Reinforced Concrete Frames.* Kenneth John Elwood and Jack P. Moehle. November 2003.
- PEER 2002/24** *Performance of Beam to Column Bridge Joints Subjected to a Large Velocity Pulse.* Natalie Gibson, André Filiatrault, and Scott A. Ashford. April 2002.
- PEER 2002/23** *Effects of Large Velocity Pulses on Reinforced Concrete Bridge Columns.* Greg L. Orozco and Scott A. Ashford. April 2002.
- PEER 2002/22** *Characterization of Large Velocity Pulses for Laboratory Testing.* Kenneth E. Cox and Scott A. Ashford. April 2002.
- PEER 2002/21** *Fourth U.S.-Japan Workshop on Performance-Based Earthquake Engineering Methodology for Reinforced Concrete Building Structures.* December 2002.
- PEER 2002/20** *Barriers to Adoption and Implementation of PBEE Innovations.* Peter J. May. August 2002.
- PEER 2002/19** *Economic-Engineered Integrated Models for Earthquakes: Socioeconomic Impacts.* Peter Gordon, James E. Moore II, and Harry W. Richardson. July 2002.
- PEER 2002/18** *Assessment of Reinforced Concrete Building Exterior Joints with Substandard Details.* Chris P. Pantelides, Jon Hansen, Justin Nadauld, and Lawrence D. Reaveley. May 2002.
- PEER 2002/17** *Structural Characterization and Seismic Response Analysis of a Highway Overcrossing Equipped with Elastomeric Bearings and Fluid Dampers: A Case Study.* Nicos Makris and Jian Zhang. November 2002.
- PEER 2002/16** *Estimation of Uncertainty in Geotechnical Properties for Performance-Based Earthquake Engineering.* Allen L. Jones, Steven L. Kramer, and Pedro Arduino. December 2002.
- PEER 2002/15** *Seismic Behavior of Bridge Columns Subjected to Various Loading Patterns.* Asadollah Esmaeily-Gh. and Yan Xiao. December 2002.
- PEER 2002/14** *Inelastic Seismic Response of Extended Pile Shaft Supported Bridge Structures.* T.C. Hutchinson, R.W. Boulanger, Y.H. Chai, and I.M. Idriss. December 2002.
- PEER 2002/13** *Probabilistic Models and Fragility Estimates for Bridge Components and Systems.* Paolo Gardoni, Armen Der Kiureghian, and Khalid M. Mosalam. June 2002.
- PEER 2002/12** *Effects of Fault Dip and Slip Rake on Near-Source Ground Motions: Why Chi-Chi Was a Relatively Mild M7.6 Earthquake.* Brad T. Aagaard, John F. Hall, and Thomas H. Heaton. December 2002.
- PEER 2002/11** *Analytical and Experimental Study of Fiber-Reinforced Strip Isolators.* James M. Kelly and Shakhzod M. Takhirov. September 2002.
- PEER 2002/10** *Centrifuge Modeling of Settlement and Lateral Spreading with Comparisons to Numerical Analyses.* Sivapalan Gajan and Bruce L. Kutter. January 2003.
- PEER 2002/09** *Documentation and Analysis of Field Case Histories of Seismic Compression during the 1994 Northridge, California, Earthquake.* Jonathan P. Stewart, Patrick M. Smith, Daniel H. Whang, and Jonathan D. Bray. October 2002.
- PEER 2002/08** *Component Testing, Stability Analysis and Characterization of Buckling-Restrained Unbonded Braces™.* Cameron Black, Nicos Makris, and Ian Aiken. September 2002.
- PEER 2002/07** *Seismic Performance of Pile-Wharf Connections.* Charles W. Roeder, Robert Graff, Jennifer Soderstrom, and Jun Han Yoo. December 2001.
- PEER 2002/06** *The Use of Benefit-Cost Analysis for Evaluation of Performance-Based Earthquake Engineering Decisions.* Richard O. Zerbe and Anthony Falit-Baiamonte. September 2001.
- PEER 2002/05** *Guidelines, Specifications, and Seismic Performance Characterization of Nonstructural Building Components and Equipment.* André Filiatrault, Constantin Christopoulos, and Christopher Stearns. September 2001.
- PEER 2002/04** *Consortium of Organizations for Strong-Motion Observation Systems and the Pacific Earthquake Engineering Research Center Lifelines Program: Invited Workshop on Archiving and Web Dissemination of Geotechnical Data, 4–5 October 2001.* September 2002.
- PEER 2002/03** *Investigation of Sensitivity of Building Loss Estimates to Major Uncertain Variables for the Van Nuys Testbed.* Keith A. Porter, James L. Beck, and Rustem V. Shaikhutdinov. August 2002.

- PEER 2002/02** *The Third U.S.-Japan Workshop on Performance-Based Earthquake Engineering Methodology for Reinforced Concrete Building Structures.* July 2002.
- PEER 2002/01** *Nonstructural Loss Estimation: The UC Berkeley Case Study.* Mary C. Comerio and John C. Stallmeyer. December 2001.
- PEER 2001/16** *Statistics of SDF-System Estimate of Roof Displacement for Pushover Analysis of Buildings.* Anil K. Chopra, Rakesh K. Goel, and Chatpan Chintanapakdee. December 2001.
- PEER 2001/15** *Damage to Bridges during the 2001 Nisqually Earthquake.* R. Tyler Ranf, Marc O. Eberhard, and Michael P. Berry. November 2001.
- PEER 2001/14** *Rocking Response of Equipment Anchored to a Base Foundation.* Nicos Makris and Cameron J. Black. September 2001.
- PEER 2001/13** *Modeling Soil Liquefaction Hazards for Performance-Based Earthquake Engineering.* Steven L. Kramer and Ahmed-W. Elgamal. February 2001.
- PEER 2001/12** *Development of Geotechnical Capabilities in OpenSees.* Boris Jeremić. September 2001.
- PEER 2001/11** *Analytical and Experimental Study of Fiber-Reinforced Elastomeric Isolators.* James M. Kelly and Shakhzod M. Takhirov. September 2001.
- PEER 2001/10** *Amplification Factors for Spectral Acceleration in Active Regions.* Jonathan P. Stewart, Andrew H. Liu, Yoojoong Choi, and Mehmet B. Baturay. December 2001.
- PEER 2001/09** *Ground Motion Evaluation Procedures for Performance-Based Design.* Jonathan P. Stewart, Shyh-Jeng Chiou, Jonathan D. Bray, Robert W. Graves, Paul G. Somerville, and Norman A. Abrahamson. September 2001.
- PEER 2001/08** *Experimental and Computational Evaluation of Reinforced Concrete Bridge Beam-Column Connections for Seismic Performance.* Clay J. Naito, Jack P. Moehle, and Khalid M. Mosalam. November 2001.
- PEER 2001/07** *The Rocking Spectrum and the Shortcomings of Design Guidelines.* Nicos Makris and Dimitrios Konstantinidis. August 2001.
- PEER 2001/06** *Development of an Electrical Substation Equipment Performance Database for Evaluation of Equipment Fragilities.* Thalia Agnanos. April 1999.
- PEER 2001/05** *Stiffness Analysis of Fiber-Reinforced Elastomeric Isolators.* Hsiang-Chuan Tsai and James M. Kelly. May 2001.
- PEER 2001/04** *Organizational and Societal Considerations for Performance-Based Earthquake Engineering.* Peter J. May. April 2001.
- PEER 2001/03** *A Modal Pushover Analysis Procedure to Estimate Seismic Demands for Buildings: Theory and Preliminary Evaluation.* Anil K. Chopra and Rakesh K. Goel. January 2001.
- PEER 2001/02** *Seismic Response Analysis of Highway Overcrossings Including Soil-Structure Interaction.* Jian Zhang and Nicos Makris. March 2001.
- PEER 2001/01** *Experimental Study of Large Seismic Steel Beam-to-Column Connections.* Egor P. Popov and Shakhzod M. Takhirov. November 2000.
- PEER 2000/10** *The Second U.S.-Japan Workshop on Performance-Based Earthquake Engineering Methodology for Reinforced Concrete Building Structures.* March 2000.
- PEER 2000/09** *Structural Engineering Reconnaissance of the August 17, 1999 Earthquake: Kocaeli (Izmit), Turkey.* Halil Sezen, Kenneth J. Elwood, Andrew S. Whittaker, Khalid Mosalam, John J. Wallace, and John F. Stanton. December 2000.
- PEER 2000/08** *Behavior of Reinforced Concrete Bridge Columns Having Varying Aspect Ratios and Varying Lengths of Confinement.* Anthony J. Calderone, Dawn E. Lehman, and Jack P. Moehle. January 2001.
- PEER 2000/07** *Cover-Plate and Flange-Plate Reinforced Steel Moment-Resisting Connections.* Taejin Kim, Andrew S. Whittaker, Amir S. Gilani, Vitelmo V. Bertero, and Shakhzod M. Takhirov. September 2000.
- PEER 2000/06** *Seismic Evaluation and Analysis of 230-kV Disconnect Switches.* Amir S. J. Gilani, Andrew S. Whittaker, Gregory L. Fennes, Chun-Hao Chen, Henry Ho, and Eric Fujisaki. July 2000.
- PEER 2000/05** *Performance-Based Evaluation of Exterior Reinforced Concrete Building Joints for Seismic Excitation.* Chandra Clyde, Chris P. Pantelides, and Lawrence D. Reaveley. July 2000.
- PEER 2000/04** *An Evaluation of Seismic Energy Demand: An Attenuation Approach.* Chung-Che Chou and Chia-Ming Uang. July 1999.
- PEER 2000/03** *Framing Earthquake Retrofitting Decisions: The Case of Hillside Homes in Los Angeles.* Detlof von Winterfeldt, Nels Roselund, and Alicia Kitsuse. March 2000.

- PEER 2000/02** *U.S.-Japan Workshop on the Effects of Near-Field Earthquake Shaking.* Andrew Whittaker, ed. July 2000.
- PEER 2000/01** *Further Studies on Seismic Interaction in Interconnected Electrical Substation Equipment.* Armen Der Kiureghian, Kee-Jeung Hong, and Jerome L. Sackman. November 1999.
- PEER 1999/14** *Seismic Evaluation and Retrofit of 230-kV Porcelain Transformer Bushings.* Amir S. Gilani, Andrew S. Whittaker, Gregory L. Fenves, and Eric Fujisaki. December 1999.
- PEER 1999/13** *Building Vulnerability Studies: Modeling and Evaluation of Tilt-up and Steel Reinforced Concrete Buildings.* John W. Wallace, Jonathan P. Stewart, and Andrew S. Whittaker, editors. December 1999.
- PEER 1999/12** *Rehabilitation of Nonductile RC Frame Building Using Encasement Plates and Energy-Dissipating Devices.* Mehrdad Sasani, Vitelmo V. Bertero, James C. Anderson. December 1999.
- PEER 1999/11** *Performance Evaluation Database for Concrete Bridge Components and Systems under Simulated Seismic Loads.* Yael D. Hose and Frieder Seible. November 1999.
- PEER 1999/10** *U.S.-Japan Workshop on Performance-Based Earthquake Engineering Methodology for Reinforced Concrete Building Structures.* December 1999.
- PEER 1999/09** *Performance Improvement of Long Period Building Structures Subjected to Severe Pulse-Type Ground Motions.* James C. Anderson, Vitelmo V. Bertero, and Raul Bertero. October 1999.
- PEER 1999/08** *Envelopes for Seismic Response Vectors.* Charles Menun and Armen Der Kiureghian. July 1999.
- PEER 1999/07** *Documentation of Strengths and Weaknesses of Current Computer Analysis Methods for Seismic Performance of Reinforced Concrete Members.* William F. Cofer. November 1999.
- PEER 1999/06** *Rocking Response and Overturning of Anchored Equipment under Seismic Excitations.* Nicos Makris and Jian Zhang. November 1999.
- PEER 1999/05** *Seismic Evaluation of 550 kV Porcelain Transformer Bushings.* Amir S. Gilani, Andrew S. Whittaker, Gregory L. Fenves, and Eric Fujisaki. October 1999.
- PEER 1999/04** *Adoption and Enforcement of Earthquake Risk-Reduction Measures.* Peter J. May, Raymond J. Burby, T. Jens Feeley, and Robert Wood.
- PEER 1999/03** *Task 3 Characterization of Site Response General Site Categories.* Adrian Rodriguez-Marek, Jonathan D. Bray, and Norman Abrahamson. February 1999.
- PEER 1999/02** *Capacity-Demand-Diagram Methods for Estimating Seismic Deformation of Inelastic Structures: SDF Systems.* Anil K. Chopra and Rakesh Goel. April 1999.
- PEER 1999/01** *Interaction in Interconnected Electrical Substation Equipment Subjected to Earthquake Ground Motions.* Armen Der Kiureghian, Jerome L. Sackman, and Kee-Jeung Hong. February 1999.
- PEER 1998/08** *Behavior and Failure Analysis of a Multiple-Frame Highway Bridge in the 1994 Northridge Earthquake.* Gregory L. Fenves and Michael Ellery. December 1998.
- PEER 1998/07** *Empirical Evaluation of Inertial Soil-Structure Interaction Effects.* Jonathan P. Stewart, Raymond B. Seed, and Gregory L. Fenves. November 1998.
- PEER 1998/06** *Effect of Damping Mechanisms on the Response of Seismic Isolated Structures.* Nicos Makris and Shih-Po Chang. November 1998.
- PEER 1998/05** *Rocking Response and Overturning of Equipment under Horizontal Pulse-Type Motions.* Nicos Makris and Yiannis Roussos. October 1998.
- PEER 1998/04** *Pacific Earthquake Engineering Research Invitational Workshop Proceedings, May 14–15, 1998: Defining the Links between Planning, Policy Analysis, Economics and Earthquake Engineering.* Mary Comerio and Peter Gordon. September 1998.
- PEER 1998/03** *Repair/Upgrade Procedures for Welded Beam to Column Connections.* James C. Anderson and Xiaojing Duan. May 1998.
- PEER 1998/02** *Seismic Evaluation of 196 kV Porcelain Transformer Bushings.* Amir S. Gilani, Juan W. Chavez, Gregory L. Fenves, and Andrew S. Whittaker. May 1998.
- PEER 1998/01** *Seismic Performance of Well-Confined Concrete Bridge Columns.* Dawn E. Lehman and Jack P. Moehle. December 2000.

ONLINE PEER REPORTS

The following PEER reports are available by Internet only at http://peer.berkeley.edu/publications/peer_reports_complete.html.

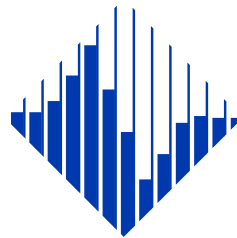
- PEER 2012/103** *Performance-Based Seismic Demand Assessment of Concentrically Braced Steel Frame Buildings*. Chui-Hsin Chen and Stephen A. Mahin. December 2012.
- PEER 2012/102** *Procedure to Restart an Interrupted Hybrid Simulation: Addendum to PEER Report 2010/103*. Vesna Terzic and Božidar Stojadinovic. October 2012.
- PEER 2012/101** *Mechanics of Fiber Reinforced Bearings*. James M. Kelly and Andrea Calabrese. February 2012.
- PEER 2011/107** *Nonlinear Site Response and Seismic Compression at Vertical Array Strongly Shaken by 2007 Niigata-ken Chuetsu-oki Earthquake*. Eric Yee, Jonathan P. Stewart, and Kohji Tokimatsu. December 2011.
- PEER 2011/106** *Self Compacting Hybrid Fiber Reinforced Concrete Composites for Bridge Columns*. Pardeep Kumar, Gabriel Jen, William Trono, Marios Panagiotou, and Claudia Ostertag. September 2011.
- PEER 2011/105** *Stochastic Dynamic Analysis of Bridges Subjected to Spatially Varying Ground Motions*. Katerina Konakli and Armen Der Kiureghian. August 2011.
- PEER 2011/104** *Design and Instrumentation of the 2010 E-Defense Four-Story Reinforced Concrete and Post-Tensioned Concrete Buildings*. Takuya Nagae, Kenichi Tahara, Taizo Matsumori, Hitoshi Shiohara, Toshimi Kabeyasawa, Susumu Kono, Minehiro Nishiyama (Japanese Research Team) and John Wallace, Wassim Ghannoum, Jack Moehle, Richard Sause, Wesley Keller, Zeynep Tuna (U.S. Research Team). June 2011.
- PEER 2011/103** *In-Situ Monitoring of the Force Output of Fluid Dampers: Experimental Investigation*. Dimitrios Konstantinidis, James M. Kelly, and Nicos Makris. April 2011.
- PEER 2011/102** *Ground-motion prediction equations 1964 - 2010*. John Douglas. April 2011.
- PEER 2011/101** *Report of the Eighth Planning Meeting of NEES/E-Defense Collaborative Research on Earthquake Engineering*. Convened by the Hyogo Earthquake Engineering Research Center (NIED), NEES Consortium, Inc. February 2011.
- PEER 2010/111** *Modeling and Acceptance Criteria for Seismic Design and Analysis of Tall Buildings*. Task 7 Report for the Tall Buildings Initiative - Published jointly by the Applied Technology Council. October 2010.
- PEER 2010/110** *Seismic Performance Assessment and Probabilistic Repair Cost Analysis of Precast Concrete Cladding Systems for Multistory Buildings*. Jeffrey P. Hunt and Božidar Stojadinovic. November 2010.
- PEER 2010/109** *Report of the Seventh Joint Planning Meeting of NEES/E-Defense Collaboration on Earthquake Engineering. Held at the E-Defense, Miki, and Shin-Kobe, Japan, September 18–19, 2009*. August 2010.
- PEER 2010/108** *Probabilistic Tsunami Hazard in California*. Hong Kie Thio, Paul Somerville, and Jascha Polet, preparers. October 2010.
- PEER 2010/107** *Performance and Reliability of Exposed Column Base Plate Connections for Steel Moment-Resisting Frames*. Ady Aviram, Božidar Stojadinovic, and Armen Der Kiureghian. August 2010.
- PEER 2010/106** *Verification of Probabilistic Seismic Hazard Analysis Computer Programs*. Patricia Thomas, Ivan Wong, and Norman Abrahamson. May 2010.
- PEER 2010/105** *Structural Engineering Reconnaissance of the April 6, 2009, Abruzzo, Italy, Earthquake, and Lessons Learned*. M. Selim Günay and Khalid M. Mosalam. April 2010.
- PEER 2010/104** *Simulating the Inelastic Seismic Behavior of Steel Braced Frames, Including the Effects of Low-Cycle Fatigue*. Yuli Huang and Stephen A. Mahin. April 2010.
- PEER 2010/103** *Post-Earthquake Traffic Capacity of Modern Bridges in California*. Vesna Terzic and Božidar Stojadinović. March 2010.
- PEER 2010/102** *Analysis of Cumulative Absolute Velocity (CAV) and JMA Instrumental Seismic Intensity (I_{JMA}) Using the PEER-NGA Strong Motion Database*. Kenneth W. Campbell and Yousef Bozorgnia. February 2010.
- PEER 2010/101** *Rocking Response of Bridges on Shallow Foundations*. Jose A. Ugalde, Bruce L. Kutter, and Boris Jeremic. April 2010.
- PEER 2009/109** *Simulation and Performance-Based Earthquake Engineering Assessment of Self-Centering Post-Tensioned Concrete Bridge Systems*. Won K. Lee and Sarah L. Billington. December 2009.
- PEER 2009/108** *PEER Lifelines Geotechnical Virtual Data Center*. J. Carl Stepp, Daniel J. Ponti, Loren L. Turner, Jennifer N. Swift, Sean Devlin, Yang Zhu, Jean Benoit, and John Bobbitt. September 2009.
- PEER 2009/107** *Experimental and Computational Evaluation of Current and Innovative In-Span Hinge Details in Reinforced Concrete Box-Girder Bridges: Part 2: Post-Test Analysis and Design Recommendations*. Matias A. Hube and Khalid M. Mosalam. December 2009.

- PEER 2009/106** *Shear Strength Models of Exterior Beam-Column Joints without Transverse Reinforcement.* Sangjoon Park and Khalid M. Mosalam. November 2009.
- PEER 2009/105** *Reduced Uncertainty of Ground Motion Prediction Equations through Bayesian Variance Analysis.* Robb Eric S. Moss. November 2009.
- PEER 2009/104** *Advanced Implementation of Hybrid Simulation.* Andreas H. Schellenberg, Stephen A. Mahin, Gregory L. Fenves. November 2009.
- PEER 2009/103** *Performance Evaluation of Innovative Steel Braced Frames.* T. Y. Yang, Jack P. Moehle, and Božidar Stojadinovic. August 2009.
- PEER 2009/102** *Reinvestigation of Liquefaction and Nonliquefaction Case Histories from the 1976 Tangshan Earthquake.* Robb Eric Moss, Robert E. Kayen, Liyuan Tong, Songyu Liu, Guojun Cai, and Jiaer Wu. August 2009.
- PEER 2009/101** *Report of the First Joint Planning Meeting for the Second Phase of NEES/E-Defense Collaborative Research on Earthquake Engineering.* Stephen A. Mahin et al. July 2009.
- PEER 2008/104** *Experimental and Analytical Study of the Seismic Performance of Retaining Structures.* Linda Al Atik and Nicholas Sitar. January 2009.
- PEER 2008/103** *Experimental and Computational Evaluation of Current and Innovative In-Span Hinge Details in Reinforced Concrete Box-Girder Bridges. Part 1: Experimental Findings and Pre-Test Analysis.* Matias A. Hube and Khalid M. Mosalam. January 2009.
- PEER 2008/102** *Modeling of Unreinforced Masonry Infill Walls Considering In-Plane and Out-of-Plane Interaction.* Stephen Kadysiewski and Khalid M. Mosalam. January 2009.
- PEER 2008/101** *Seismic Performance Objectives for Tall Buildings.* William T. Holmes, Charles Kircher, William Petak, and Nabih Youssef. August 2008.
- PEER 2007/101** *Generalized Hybrid Simulation Framework for Structural Systems Subjected to Seismic Loading.* Tarek Elkhoraibi and Khalid M. Mosalam. July 2007.
- PEER 2007/100** *Seismic Evaluation of Reinforced Concrete Buildings Including Effects of Masonry Infill Walls.* Alidad Hashemi and Khalid M. Mosalam. July 2007.

The Pacific Earthquake Engineering Research Center (PEER) is a multi-institutional research and education center with headquarters at the University of California, Berkeley. Investigators from over 20 universities, several consulting companies, and researchers at various state and federal government agencies contribute to research programs focused on performance-based earthquake engineering.

These research programs aim to identify and reduce the risks from major earthquakes to life safety and to the economy by including research in a wide variety of disciplines including structural and geotechnical engineering, geology/seismology, lifelines, transportation, architecture, economics, risk management, and public policy.

PEER is supported by federal, state, local, and regional agencies, together with industry partners.



PEER Core Institutions:
University of California, Berkeley (Lead Institution)
California Institute of Technology
Oregon State University
Stanford University
University of California, Davis
University of California, Irvine
University of California, Los Angeles
University of California, San Diego
University of Southern California
University of Washington

PEER reports can be ordered at http://peer.berkeley.edu/publications/peer_reports.html or by contacting

Pacific Earthquake Engineering Research Center
University of California, Berkeley
325 Davis Hall, mail code 1792
Berkeley, CA 94720-1792
Tel: 510-642-3437
Fax: 510-642-1655
Email: peer_editor@berkeley.edu

ISSN 1547-0587X